Forest Ecology and Management 315 (2014) 30–42

Contents lists available at ScienceDirect

Forest Ecology and Management

journal homepage: www.elsevier.com/locate/foreco

Modeling climate and fuel reduction impacts on mixed-conifer forest carbon stocks in the Sierra Nevada, California

Matthew D. Hurteau [a,*], Timothy A. Robards [b], Donald Stevens [c], David Saah [b,d], Malcolm North [e], George W. Koch [c,f]

[a] Department of Ecosystem Science and Management, The Pennsylvania State University, 306 Forest Resources Building, University Park, PA 16802, United States
[b] Spatial Informatics Group, LLC, 3248 Northampton Ct, Pleasanton, CA 94588, United States
[c] Merriam-Powell Center for Environmental Research, Northern Arizona University, Flagstaff, AZ 86011, United States
[d] Department of Environmental Science, University of San Francisco, San Francisco, CA 94117, United States
[e] USDA Forest Service, Pacific Southwest Research Station, 1731 Research Park Dr., Davis, CA 95618, United States
[f] Department of Biological Sciences, Northern Arizona University, Flagstaff, AZ 86011, United States

ARTICLE INFO

Article history:
Received 25 October 2013
Received in revised form 13 December 2013
Accepted 14 December 2013
Available online 9 January 2014

Keywords:
Climate change
Growth-and-yield
Mitigation
Thinning
Wildfire
Adaptation

ABSTRACT

Quantifying the impacts of changing climatic conditions on forest growth is integral to estimating future forest carbon balance. We used a growth-and-yield model, modified for climate sensitivity, to quantify the effects of altered climate on mixed-conifer forest growth in the Lake Tahoe Basin, California. Estimates of forest growth and live tree carbon stocks were made for low and high emission scenarios using four downscaled general circulation model (GCM) projections. The climate scenarios were coupled with a range of commonly-used fuels reduction treatments to quantify the combined effects of these factors on live tree carbon stocks. We compared mid- (2020–2049) and late-21st (2070–2099) century carbon stock estimates with a baseline period of 1970–1999 using common input data across time periods. Recursive partitioning analysis indicates that GCM, forest composition, and simulation period most influence live tree carbon stock changes. Comparison with the late 20th century baseline period shows mixed carbon stock responses across scenarios. Growth varied by species, often with compensatory responses among dominant species that limited changes in total live tree carbon. The influence of wildfire mitigation treatments was relatively consistent with each GCM by emission scenario combination. Treatments that included prescribed fire had greater live tree carbon gains relative to baseline under the scenarios that had overall live tree carbon gains. However, across GCMs the influence of treatments varied considerably among GCM projections, indicating that further refinement of regional climate projections will be required to improve model estimates of fuel manipulations on forest carbon stocks. Additionally, had out simulations included the effects of projected climate changes on increasing wildfire probability, the effects of management treatments on carbon stocks may have been more pronounced because of the influence of treatment on fire severity.

© 2013 Elsevier B.V. All rights reserved.

1. Introduction

Management of forest-based carbon sequestration represents part of the portfolio of current technologies that can be implemented to mitigate changing climatic conditions (Pacala and Socolow, 2004). This can take the form of reducing deforestation, increasing carbon density, afforestation/reforestation, or replacing fossil-based energy sources with sustainably-harvested forest biomass (Canadell and Raupach, 2008). While forest-based climate change mitigation does offer promise, especially with regards to reducing tropical deforestation (Gullison et al., 2007), it is not without risk (Galik and Jackson, 2009).

Risk is commonly defined as the product of the probability of an event occurring and the consequence of that event. In the case of forest carbon loss due to wildfire, the consequence is a function of fire effects on the forest (Hurteau et al., 2013). High-severity fire causes greater carbon loss than low-severity fire, resulting in a larger consequence (Hurteau and Brooks, 2011). Fire effects on the forest can be managed by altering forest structure and fuel loads, thereby reducing the risk of carbon loss due to wildfire (Hurteau et al., 2009). However, this risk reduction measure carries a carbon stock reduction cost and the carbon balance of a specific treatment is dependent upon a wildfire burning in the treated area, the end-use of the trees harvested during treatment, among other factors (Mitchell et al., 2009; North et al., 2009; Stephens et al., 2009b; Hurteau et al., 2011; Campbell et al., 2012; Winford and Gaither, 2012). Generally, the probability of a fire event occurring at most

* Corresponding author. Tel.: +1 (814) 865 7554; fax: +1 (814) 865 3725.
E-mail address: matthew.hurteau@psu.edu (M.D. Hurteau).

0378-1127/$ - see front matter © 2013 Elsevier B.V. All rights reserved.
http://dx.doi.org/10.1016/j.foreco.2013.12.012

forest locations in any given year is quite low (Dickson et al., 2006). However, warming temperatures are increasing the frequency of large wildfires (Westerling and Bryant, 2008; Pechony and Shindell, 2010; Westerling et al., 2011) and may also increase fire severity. Based on two general circulation model projections under a doubling of atmospheric CO_2, Flannigan et al. (2000) projected that mean fire severity in California (measured by difficulty of control) would increase by about 10% averaged across the state by mid-century. Results from Lenihan et al. (2003, 2008) suggest that large proportions of the Sierra Nevada landscape may experience an increase in mean fire intensity over current conditions by the end of the century, depending on future precipitation patterns. Therefore, the risk of carbon loss due to wildfire is likely to increase as a function of the increasing probability and severity of wildfire.

The carbon carrying capacity of a system has been defined as the amount of carbon that can be sustained under prevailing climatic conditions and natural disturbance regimes (Keith et al., 2009). Human intervention in the form of fire exclusion has resulted in a carbon density that exceeds the carrying capacity in some systems, with the result being a proportionately greater carbon loss when wildfire occurs (Dore et al., 2008; Hurteau et al., 2011). In addition to altering forest structure, fire exclusion has also impacted forest composition. In the mixed-conifer forests of the Sierra Nevada of California, fire-exclusion has resulted in increased tree density, decreased mean diameter, and a greater proportion of the basal area being comprised of fire-sensitive species (North et al., 2007). The pulse of post-fire-exclusion recruitment of these species (e.g. *Abies concolor* and *Calocedrus decurrens*) coincided with a climatic shift to warmer and wetter conditions (North et al., 2005; Beaty and Taylor, 2008). While it is difficult to discern the exact cause of this change in species composition, it raises the question of how a shift to even warmer conditions, with increased fire frequency and altered precipitation, will influence the carbon carrying capacity of forests.

In addition to influencing disturbance, changes in climate can impact forest growth and mortality, contributing uncertainty to the role of forests in climate change mitigation (Battles et al., 2008; vanMantgem et al., 2009). Growth-and-yield models, such as the Forest Vegetation Simulator (FVS), typically project forest growth assuming a static climate (Crookston et al., 2010). Thus, projecting forest growth under changing climatic conditions, using past climate–growth relationships has the potential to yield erroneous results. The bioclimate envelope modeling approach has been widely employed to predict how individual species ranges will change in climate space. A major criticism of this approach has been that it neglects the influence of biotic interactions on species distributions (Pearson and Dawson, 2003). One approach to overcome the short-comings of a purely climate-driven approach to modeling species-specific growth to climate is to incorporate climate sensitivity into the growth and mortality functions of models such as FVS.

The purpose of this study was to quantify the influence of predicted changes in climate on live tree carbon stocks, as a function of species-specific carbon stock changes, in a Sierran mixed-conifer forest by accounting for both biotic and abiotic influences on growth. Additionally, we sought to determine the carbon stock implications of treatments implemented to reduce the risk of high-severity wildfire and their interaction with climate impacts on growth.

2. Materials and methods

This study utilized field data to drive a climate-sensitive growth-and-yield model to project species-specific growth as a function of down-scaled climate projections from four different GCMs under two different emissions scenarios. The modeling approach used differs from climate-only approaches by incorporating biotic influences on tree growth, specifically competition. It also differs from the approach of Crookston et al. (2010) by directly incorporating climate projections, as opposed to representing changes in climate through changes in site index.

2.1. Study location

This study was conducted in the mixed-conifer forest of the Lake Tahoe Basin, California (Supplementary Fig. S1). Mixed-conifer forest occupies an elevation range from the lakeshore at 1897 m to approximately 2400 m in elevation, as a function of aspect. The forest is comprised primarily of six tree species; white fir (*A. concolor*), red fir (*A. magnifica*), incense-cedar (*C. decurrens*), Jeffrey pine (*Pinus jeffreyi*), ponderosa pine (*P. ponderosa*), and sugar pine (*P. lambertiana*). The Lake Tahoe Basin has a Mediterranean climate, with a majority of the annual precipitation (mean annual precipitation water equivalent 802 mm, National Climate Data Center, Tahoe City) falling as snow and the summers being dry and warm. The history of human impacts in the Basin includes a significant period of tree harvest during the late 1800s, when a majority of the area was logged to provide timber for Nevada's silver mining operations (Eliott-Fisk et al., 1996). Prior to the late 1800s, frequent fires in the Basin had a mean return interval ranging from 8 to 17 years in the yellow pine and mixed-conifer forest types (Beaty and Taylor, 2008).

2.2. Field data

Two to four plots were established in each of 21 creek drainages and were 1900–2200 m in elevation (Supplementary Fig. S1). Plots used in this study were selected to represent upland conditions and were co-located, approximately 150 m up-slope, with plots in the riparian zone for use in reconstructing riparian fire history (VandeWater and North, 2010). Plots located on the western side of the Basin were fir-dominated, while those located along the eastern shore were pine-dominated. Trees were sampled within plots using a nested design where all trees $\geqslant$5 cm diameter at breast height (dbh) were measured in a 1/50th ha subplot, all trees $\geqslant$50 cm dbh were measured in a 1/10th ha subplot, and all trees $\geqslant$80 cm dbh were measured in a 1/5th ha plot. Fuels were quantified along four modified Brown's transects (Brown, 1974) oriented in the cardinal directions at each plot. To assess regeneration, all trees <5 cm dbh where some portion of the tree intersected the transect were tallied by species along each fuels transect. These plot data were used to initiate model runs for each of three time periods, including a historical baseline (1970–1999), mid-century (2020–2049), and late-century (2070–2099) projections.

2.3. Model

To quantify the effects of climate and management treatment on forest growth and live tree carbon stocks we used a modified version of the Western Sierra Variant of the Forest Vegetation Simulator (Keyser, 2008). The Forest Vegetation Simulator (FVS) is a distance-independent, growth-and-yield model that can simulate a wide range of silvicultural treatments for most major forest tree species (Crookston and Dixon, 2005). The modified Western Sierra Variant of FVS (FVS-WS-CLIM) developed by Robards (2009) uses climate-sensitive, species-specific growth models and downscaled monthly climate data to model tree growth as a function of climate and management. This climate-sensitive model was developed using permanent plot and tree core data from 42,459 trees from 1378 plots on private and public lands across northern California, collected between 1958 and 1998, to calculate annual diameter

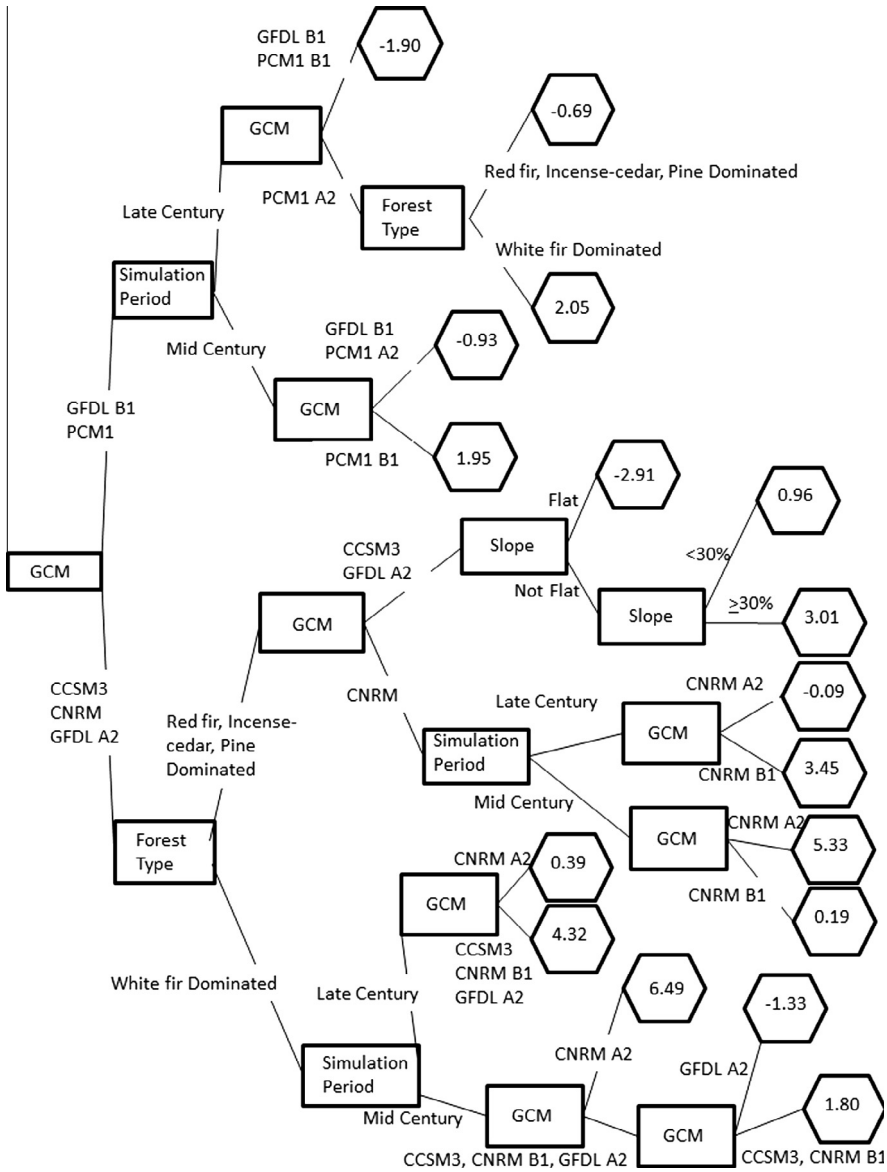

Fig. 1. Decision tree from recursive partitioning analysis to determine the most influential parameters on mean aboveground live tree carbon stocks after the mid- (2020–2049) and late-century (2070–2099) 30-year simulation periods. Terminal node values (Mg C ha^{-1}) are the difference in carbon stocks between the mid- and late-century simulation periods and the 1970–1999 baseline period.

and height growth and tree age (Supplementary Table S1). These annual measures of diameter and height growth were then used in a linear mixed effects model to develop a relationship between tree growth and a range of abiotic (e.g. elevation, slope, aspect, precipitation, and temperature) and biotic (e.g. stand density index, basal area of larger individuals, and crown ratio) factors for six conifer species; ponderosa pine, Jeffrey pine, sugar pine, incense-cedar, white fir, and red fir (Battles et al., 2008; Robards, 2009). Due to the limited availability of data for Jeffrey pine, data for this species were aggregated with ponderosa pine data, a species with which it commonly co-occurs and hybridizes (Harlow et al., 1996). Unlike the standard growth models for these species in FVS, the species-specific growth models in the modified variant include climate and topographic parameters and exclude a common parameter in growth-and-yield models, site index, which is a metric of site productivity under climatic conditions that were present during the life span of the current trees. The generalized diameter growth model structure is as follows:

$$
\begin{aligned}
E[\ln(\mathrm{GR})] = {} & b_0 + b_1 \ln(\mathrm{dbh}) + b_2(\mathrm{dbh}) + b_3\mathrm{CR} + b_4\left(\frac{\mathrm{PBAL}}{\ln(\mathrm{dbh}+1)}\right) \\
& + b_5\mathrm{PRECIP} + b_6\mathrm{TEMP} + b_7\mathrm{SL} + b_8\mathrm{SL}[\cos(\mathrm{ASP})] \\
& + b_9\mathrm{SL}[\sin(\mathrm{ASP})] + b_{10}\mathrm{SL}[\ln(\mathrm{ELEV}+1)] \\
& + b_{11}\mathrm{SL}[\ln(\mathrm{ELEV})]\cos(\mathrm{ASP}) + b_{12}\mathrm{SL}[\ln(\mathrm{ELEV}+1)] \\
& \times \sin(\mathrm{ASP}) + b_{13}\mathrm{SL}[\mathrm{ELEV}]^2 + b_{14}\mathrm{SL}[\mathrm{ELEV}]^2\cos(\mathrm{ASP}) \\
& + b_{15}\mathrm{SL}[\mathrm{ELEV}]^2\sin(\mathrm{ASP}) + b_{16}\mathrm{ELEV} + b_{17}\mathrm{ELEV}^2 \\
& + b_{18}\ \mathrm{Albrx} + b_{19}\mathrm{Albry} + e_{ik} + e
\end{aligned}
$$

where GR is the annual diameter or height growth, dbh the diameter at breast height, CR the crown ratio, PBAL the basal area in trees larger than the subject tree for a plot, SL the average slope of the plot (%), PRECIP the annual and/or seasonal precipitation (mm), TEMP the mean annual or seasonal maximum or minimum temperature (C) or number of degree days, ASP the average aspect of the plot (radians), ELEV the average elevation of the plot,

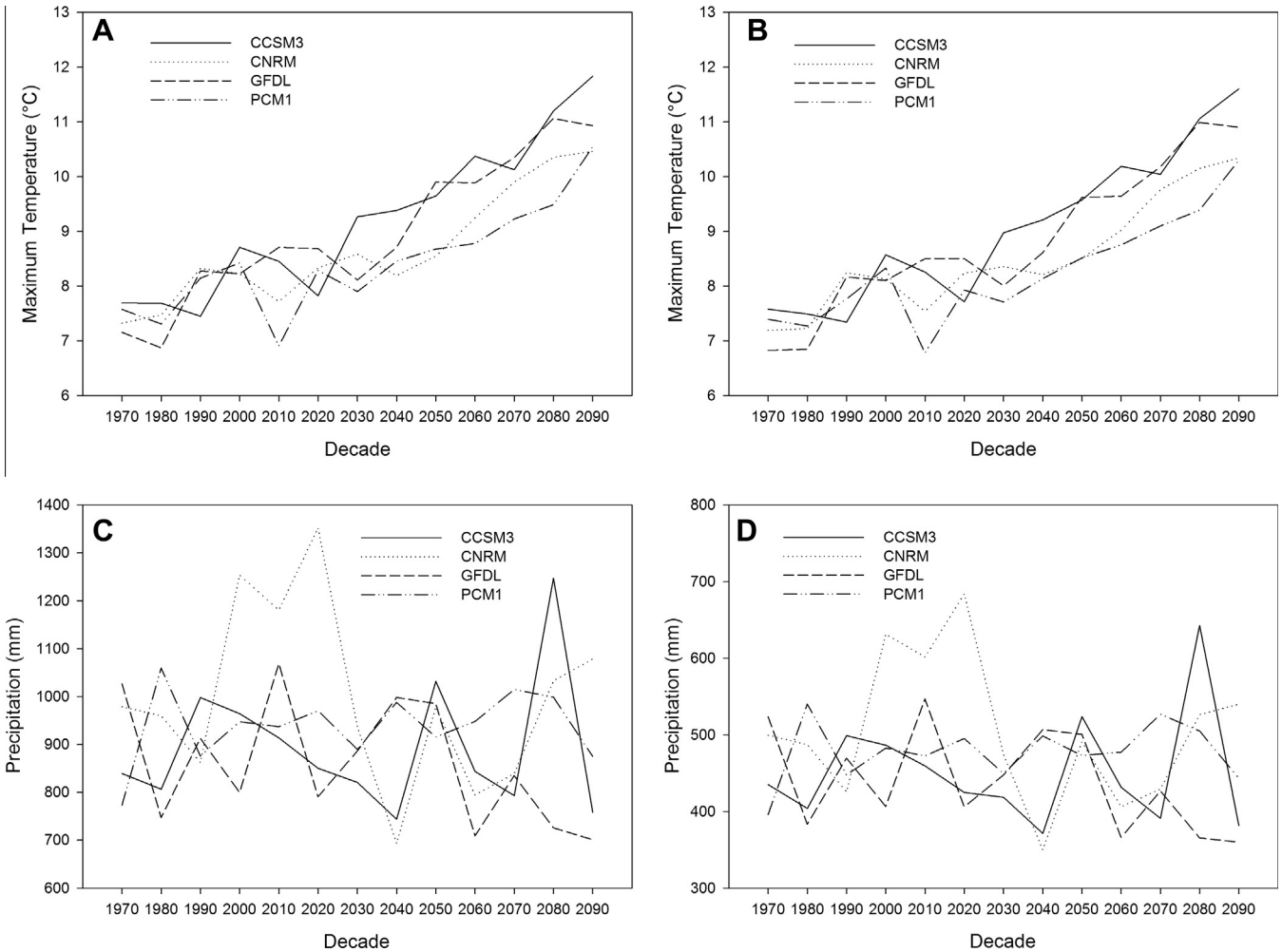

Fig. 2. Downscaled decadal mean winter maximum temperature (top row) and precipitation (bottom row) by global climate model (GCM) by decade for the western (left column) and eastern (right column) sides of the Lake Tahoe Basin. The GCM climate projections are from the National Center for Atmospheric Research Community Climate System Model (CCSM3), the Centre National de Recherches Météorologiques Coupled global Climate Model (CNRM CM3), the Geophysical Fluid Dynamics Lab coupled model (GFDL CM2.1), and the National Center for Atmospheric Research Parallel Climate Model (PCM1). The *y*-axis scale differs between panels C and D.

Albrx the longitude in UTM coordinates, Albry the latitude in UTM coordinates, e_{ik} the error of *k*th measurement on the *i*th tree, and *e* is the unexplained error.

The height growth model structure is identical to the diameter growth model with the exception that total height (tht) replaces diameter at breast height (dbh) for the variables associated with parameters b_1 and b_2. A suite of models for each species was constructed to include the range of potential parameter values (e.g. for TEMP, mean annual or seasonal maximum or minimum or number of degree days were included). Final model structure for each species was selected using the Akaike Information Criterion and Residual Maximum Likelihood Estimation (West et al., 2007) to evaluate explanatory power and parsimony. Final model parameters varied by species and height versus diameter growth (Supplementary Tables S2–S11). As an example, winter precipitation provided the most explanatory power for ponderosa pine diameter growth and winter, spring and summer precipitation provided the best fit for height growth. For sugar pine, winter precipitation was the only precipitation explanatory variable for diameter growth, while spring and summer precipitation provided the most explanatory power for height growth. Additionally, the sign of each coefficient varied by species (Supplementary Tables S12–S21). The growth models were then incorporated into the FVS model code, forming the climate sensitive variant. Model validation was conducted using tree growth data from different sites within the geographic region where the parameterization data were gathered. Modeled height and diameter were compared to empirical data for each of the four sites. These sites were located in northern, central, and southern Sierra Nevada and from the coastal mountains due west across the Central Valley. The existing FVS mortality models were retained and therefore the direct influence of climate on mortality is unaccounted. Furthermore, this approach did not account for species-specific physiological responses to changes in climate and atmospheric CO_2 concentration (see Section 4). For an in-depth description of model development, parameterization, and validation, see Robards (2009).

Downscaled monthly climate data for the Basin were assembled from the 2008 California Climate Action Team Research (12 km resolution). The climate projections were downscaled for California from four general circulation models (GCMs); GFDL CM2.1, CNRM CM3, NCAR PCM1, and NCAR CCSM3 (Hidalgo et al., 2008; Maurer and Hidalgo, 2008). The GCMs range in their responsiveness to forcing factors, with NCAR PCM1 projecting lower late-century temperature and higher precipitation than the other GCMs (Cayan et al., 2009). Two emissions scenarios were used for each of the four downscaled GCMs. The A2 scenario, with a late-century atmospheric CO_2 concentration of 850 ppm, represents continually increasing population and slower adoption of low-carbon energy sources. The B1 scenario, with late-century atmospheric CO_2 stabilization at 550 ppm, represents reduced population growth and

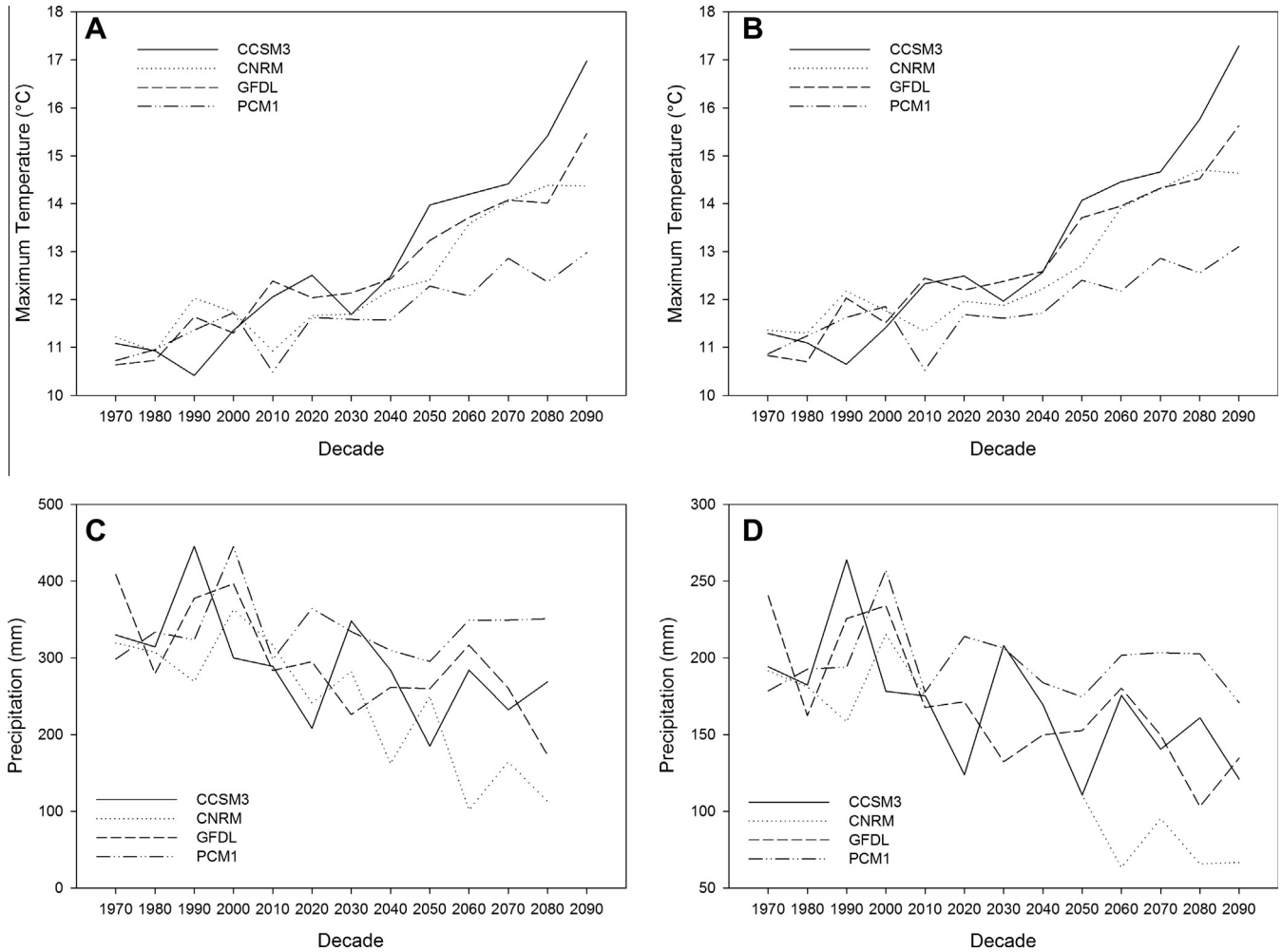

Fig. 3. Downscaled decadal mean spring maximum temperature (top row) and precipitation (bottom row) by global climate model (GCM) by decade for the western (left column) and eastern (right column) sides of the Lake Tahoe Basin. The GCM climate projections are from the National Center for Atmospheric Research Community Climate System Model (CCSM3), the Centre National de Recherches Météorologiques Coupled global Climate Model (CNRM CM3), the Geophysical Fluid Dynamics Lab coupled model (GFDL CM2.1), and the National Center for Atmospheric Research Parallel Climate Model (PCM1). The *y*-axis scale differs between panels C and D.

transition toward a low-carbon intensity economy. Model projections for mid-century and late-century temperature span 1–3 °C and 2–5 °C increases, respectively, with greater temperature increases under the A2 scenario by the end of century. Precipitation projections suggest a slight drying trend with large inter-annual variability (Cayan et al., 2009). Regardless of precipitation trends, warming across southwestern North America is likely to result in regional drying (Seager et al., 2007).

2.4. Simulations

Three simulations covering three time periods were conducted for each forest stand using FVS-WS-CLIM: a baseline simulation (1970–1999), a mid-century simulation (2020–2049), and a late-century simulation (2070–2099). Simulation periods, including the historical baseline period, used climate data from each of the four GCMs, with temperature and precipitation projections input at each time-step. Each simulation used the field data collected in 2009, inclusive of topographic position, as the starting condition. Four different management treatments were simulated for each time period: control, thin, burn, and thin and burn. The thin-only treatment involved preferentially thinning small diameter trees to a residual basal area of 28 m^2 ha^{-1} in the first year of each simulation period, based on the wildfire risk mitigation treatments often implemented in the Lake Tahoe Basin. We did not selectively thin by species. The amount of tree biomass thinned during a specific simulation was a function of the starting conditions as determined by plot-level field data. The burn-only treatment simulated a prescribed fire in the first year of each simulation period. The prescribed burns were simulated during the fall, under moist conditions (1 and 10 h fuels = 12% fuel moisture, 100 h fuels = 14%, 1000 h fuels = 25%), 21 °C air temperature, 13 kph wind speed at 6 m above ground level, with fire burning 70% of the stand area. These conditions are typical of the moderate weather conditions under which prescribed fire is often used and more easily controlled. The thin and burn treatment simulated the combination thin-from-below followed by prescribed burning during the first year of each simulation period. Background and density-induced mortality were simulated for all management treatments. Regeneration was simulated at the beginning of each period based on empirical results from similar management treatments (Zald et al., 2008). The amount of regeneration was not varied as a function of climate. Carbon stocks were estimated for aboveground live tree biomass using Forest Inventory and Analysis regional equations for volume and biomass (FIA, 2009a, b).

2.5. Analysis

The difference in carbon stocks was calculated as the projected stock minus the baseline stock at the end of the 30 year projections

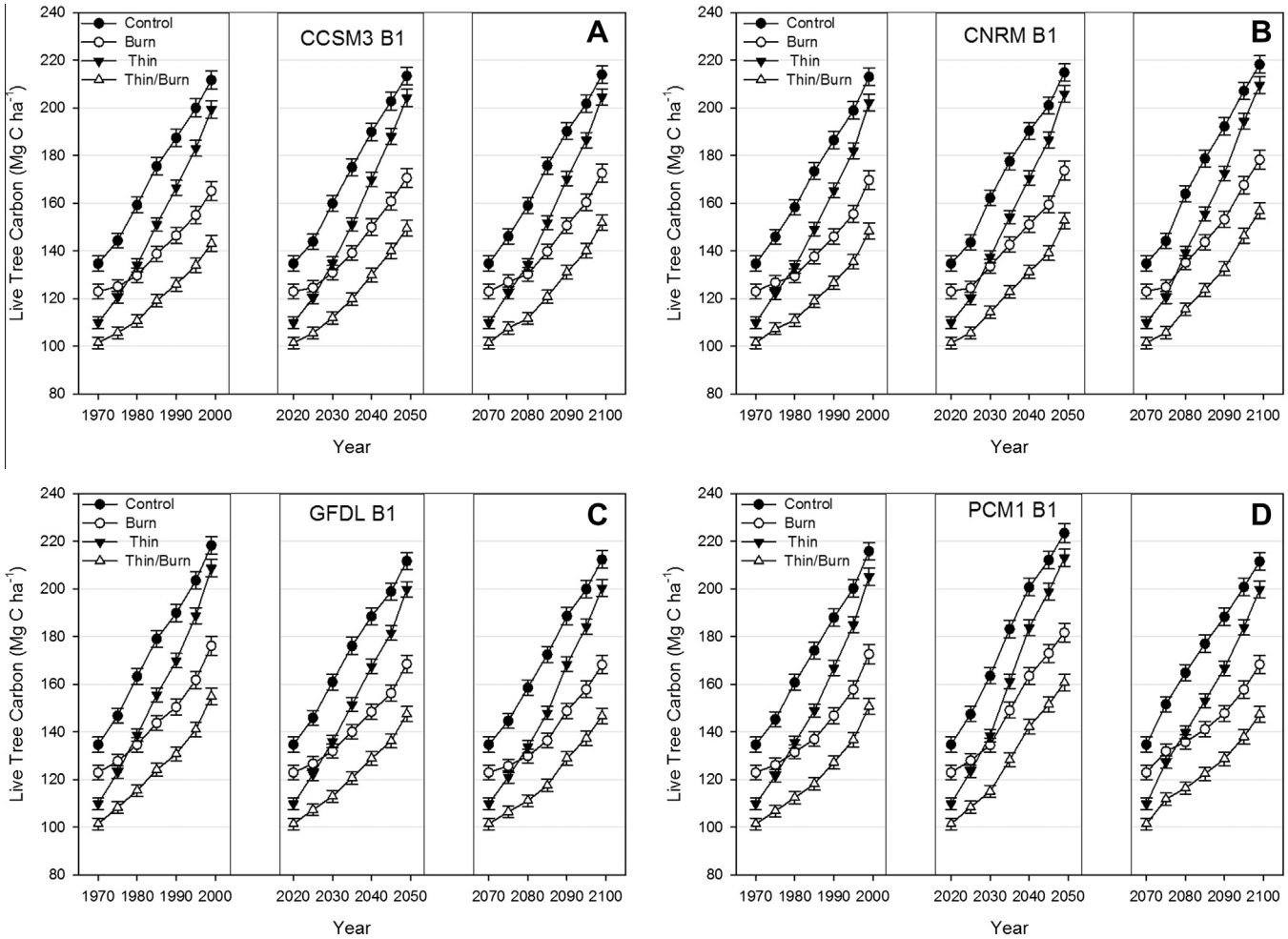

Fig. 4. Mean and standard error of live tree carbon stocks from four treatments simulated over the historical period (1970–1999), mid-century (2020–2049) and late-century (2070–2099) with climate data from four general circulation models (GCM) using the B1 emission scenario. The GCM climate projections are from the National Center for Atmospheric Research Community Climate System Model (CCSM3), the Centre National de Recherches Météorologiques Coupled global Climate Model (CNRM CM3), the Geophysical Fluid Dynamics Lab coupled model (GFDL CM2.1), and the National Center for Atmospheric Research Parallel Climate Model (PCM1). Projections are initiated using the same plot-level data.

in 2049 and 2099. Recursive partitioning of the data was conducted using default parameters and the Rpart library version 3.1–36 (Therneau et al., 2007). Recursive partitioning is a form of decision tree analysis that can be used to accurately summarize data into classes, while preserving the essential characteristics of the data (Murthy, 1998). Pruning of the resulting trees was conducted automatically using the cost-complexity prune function (Breiman et al., 1984) to minimize the cross-validated prediction error (Everitt and Hothorn, 2006). The independent variables considered were: post-treatment trees per hectare, basal area, stand density index (a commonly-used forestry metric combining stocking and basal area), time period (mid- or late-century), treatment (control, thin, burn, thin and burn), general circulation model and emission scenario, aspect, elevation, slope, Basin location (East or West), and forest type (as defined by the dominant species by basal area).

3. Results

A total of 7300 yield streams were produced from 4992 simulations (4 GCMs × 2 emission scenarios × 4 treatments × 3 time periods × 52 plots), including those for each plot and average simulations for stands. Stand-level outputs, comprised of the average of simulations from plots within a stand, numbered 2100. Outputs were produced for numbers of trees, basal area, stand density index, and carbon stock. In the recursive partitioning analysis the most influential factors were general circulation model (GCM), forest type, and simulation period (Fig. 1). The partitioning based on GCM was a function of the temperature and precipitation projections specific to each GCM-emission scenario combination. The partitioning based on simulation period was a function of projected climate over a specific time period. The projected late-century reduction in winter precipitation, an important source of moisture for tree growth, was greatest from the GFDL model under the A2 emission scenarios (Fig. 2). While all projections were for increasing temperature throughout the century, the greatest increases were from CCSM3 and GFDL (Figs. 2 and 3, Supplementary Figs. S2–S12). The partitioning based on GCM and emission scenario indicates that the level of increasing temperature and decreasing precipitation were more influential on forest carbon stock than simulation period, slope, or forest type. Slope was influential only for CCSM3 and GFDL-A2 where the dominant vegetation was not white fir. Seventeen end nodes were identified where differences between carbon stocks in 2099 and the baseline ranged from −2.91 to +6.49 Mg C ha^{-1}. The white fir-dominated forest type was consistently different from the red fir-dominated, incense-cedar-dominated and pine-dominated forest types.

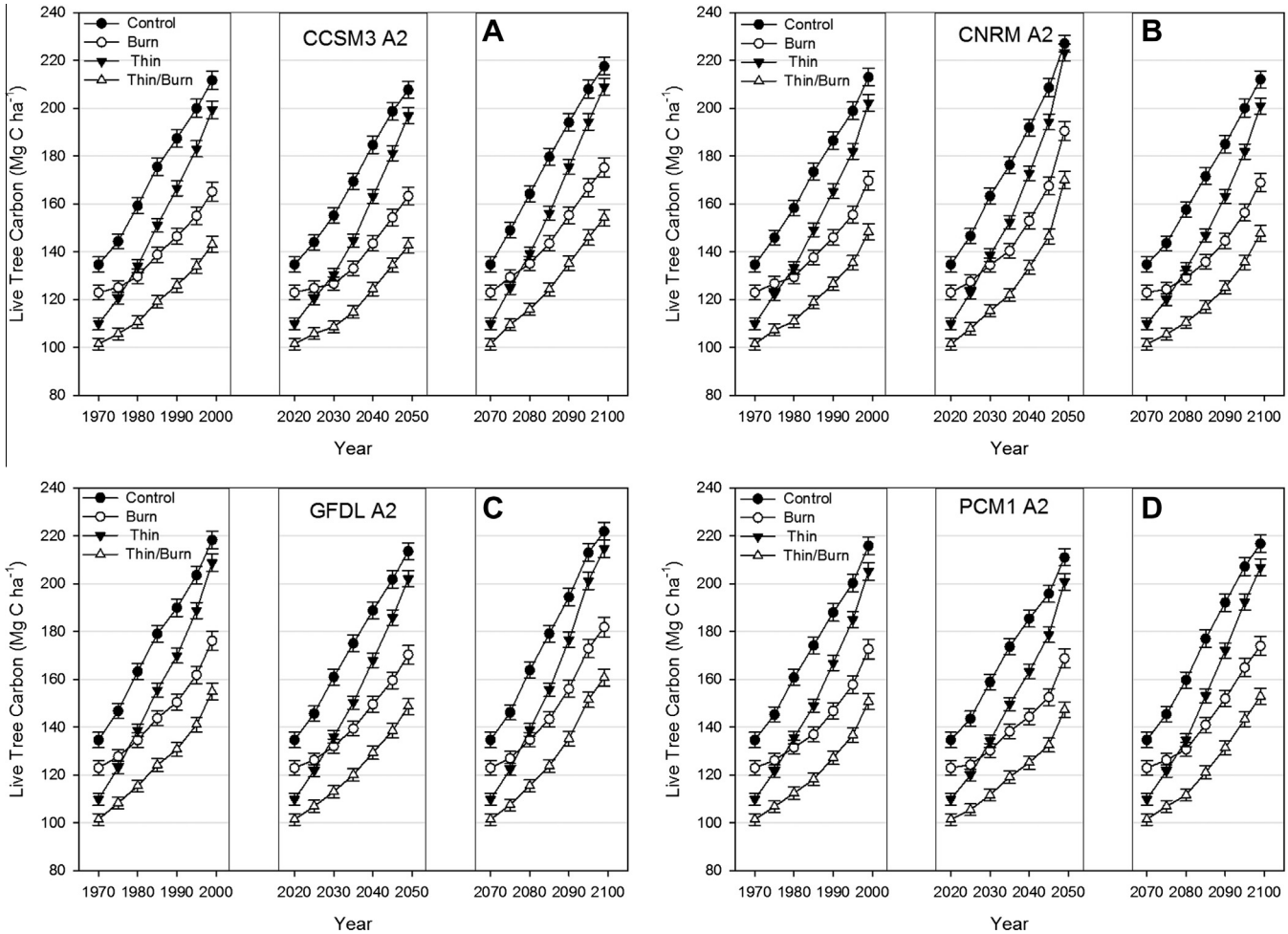

Fig. 5. Mean and standard error of live tree carbon stocks from four treatments simulated over the historical period (1970–1999), mid-century (2020–2049) and late-century (2070–2099) with climate data from four general circulation models (GCM) using the A2 emission scenario. The GCM climate projections are from the National Center for Atmospheric Research Community Climate System Model (CCSM3), the Centre National de Recherches Météorologiques Coupled global Climate Model (CNRM CM3), the Geophysical Fluid Dynamics Lab coupled model (GFDL CM2.1), and the National Center for Atmospheric Research Parallel Climate Model (PCM1). Projections are initiated using the same plot-level data.

As expected, mean live tree carbon stocks varied by treatment intensity over the baseline period (Figs. 4 and 5). The burn-only treatment resulted in the smallest initial mean decrease in live tree carbon stocks (11.7 Mg C ha^{-1}), while the thin-only (24.8 Mg C ha^{-1}) and thin and burn (33.2 Mg C ha^{-1}) had a much larger mean impact on live tree carbon, relative to the control (Figs. 4 and 5). Over the historical simulation period, the rate of increase in carbon stock size was greater in the thin-only than in the control. This increase resulted in a much smaller difference in mean thin-only carbon stocks (203.8 Mg C ha^{-1}), relative to the control (214.7 Mg C ha^{-1}) following 29 years of growth.

Carbon stocks over the mid- and late-century simulation periods varied as a function of GCM and emission scenario (Figs. 4 and 5). Across GCM, treatment means showed a slight increase over the same treatments during the baseline period for mid-century B1 projections (1.1–3.3 Mg C ha^{-1}). By late-century, across GCM treatment means showed a variable response for the B1 scenario (−0.6 to 1.4 Mg C ha^{-1}). Under the A2 scenario, mid-century across GCM treatment means also showed a slight increase (0.9–4.06 Mg C ha^{-1}). Late-century across GCM treatment means showed a larger increase for the A2 scenario (3.2–5.8 Mg C ha^{-1}). Live tree carbon stocks varied relative to baseline as a function of GCM and emission scenario. Under the B1 scenario for CCSM3, CNRM, and GFDL, live tree C stocks showed consistent directional changes relative to baseline across simulation periods (Fig. 6). Under the A2 scenario, CCSM3 and GFDL showed little change relative to baseline by the end of the mid-century simulation period. Yet, by the end of the late-century simulation period live tree carbon increased by 3.5–8.7% relative to baseline. There were two notable exceptions to these more common patterns. Mid-century, PCM1-B1 increased by 7.9–12.7% relative to baseline during the middle portion of the simulation period and by the end of the period the relative gains were roughly halved (Fig. 6). Late-century, PCM1-B1 had initial C increases and ended the simulation period with decreased live tree C relative to baseline. CNRM-A2 had the most substantial changes of all simulations during the mid-century simulation period. Relative to baseline, all treatments had increased live tree C with the largest mean gains made by the burn-only (14.5%) and thin and burn (16.9%). These two exceptions are a function of the smaller increase in temperature and decrease in precipitation projected by PCM1 and relatively small increase in warming and large mid-century increase in precipitation under CNRM-A2. Under GCM by emission scenarios where carbon stocks increased relative the baseline period, the thin and burn and burn-only treatments generally had a larger increase in live tree carbon relative to their baseline conditions, than did the control or thin-only (Fig. 6). However, in absolute terms the control and thin-only treatments consistently had larger live tree C stocks and in some

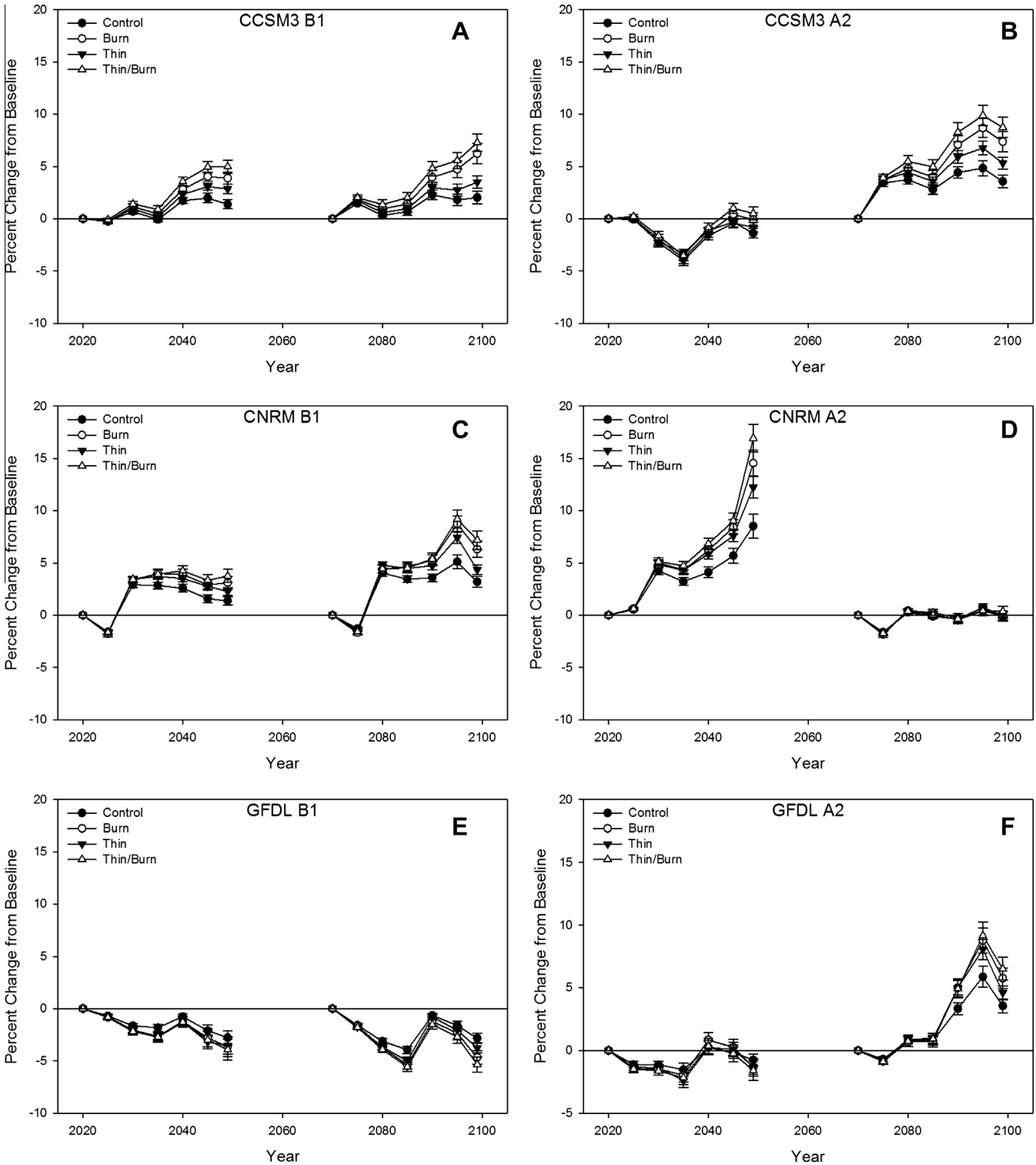

Fig. 6. Mean and standard error of percent change in live tree carbon stocks from the baseline simulation for each treatment using climate projections from four global climate models (GCM) under low (B1, left column) and high (A2, right column) emission scenarios. The GCM climate projections are from the National Center for Atmospheric Research Community Climate System Model (CCSM3), the Centre National de Recherches Météorologiques Coupled global Climate Model (CNRM CM3), the Geophysical Fluid Dynamics Lab coupled model (GFDL CM2.1), and the National Center for Atmospheric Research Parallel Climate Model (PCM1). Simulations are initiated using the same plot-level data.

cases these two treatments differ significantly by the end of the simulation period (e.g. mid-century CNRM-A2, Fig. 5).

Species specific mean live tree carbon stocks varied as a function of GCM and emission scenario projection (Tables 1 and 2). White fir and ponderosa pine are the dominant species on the west and east sides of the Basin, respectively, and had the largest changes in live tree carbon stocks of the five species modeled. Mid-century, both white fir and ponderosa pine had declines in live tree carbon, relative to the baseline, for GFDL-A2 and PCM1-A2. During the same period, both species had increases, relative to

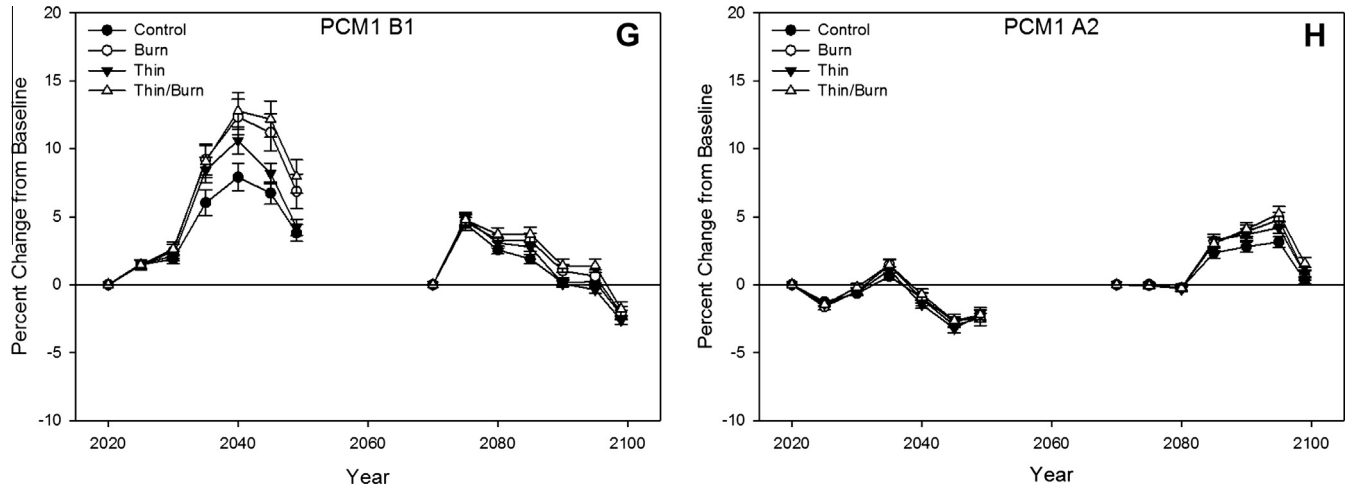

Fig. 6 (*continued*)

baseline, for PCM1-B1 and CNRM-A2. The increases for CNRM-A2 were the largest mid-century, ranging from 4.43 to 8.99 Mg C ha^{-1} for white fir and 9.52 to 10.49 Mg C ha^{-1} for ponderosa pine (Table 1). GFDL-B1 had declines in mid-century live tree carbon for the two fir species and incense-cedar, while both pine species had increases in live tree carbon (Table 1). By late-century, both white fir and ponderosa pine showed declines in live tree carbon for GFDL and PCM1 under the B1 emission scenario; yet under the A2 emission scenario, white fir live tree carbon increased under both GCMs and ponderosa pine declined. The mid-century increases in live tree carbon for both species under CNRM-A2 both became small decreases in live tree carbon, relative to baseline, by late-century. Given the limited contribution to total basal area, in general the changes from baseline were much smaller for red fir, incense-cedar, and sugar pine (Tables 1 and 2). In most cases, red fir and incense-cedar live tree carbon stocks tended to decrease relative to baseline and sugar pine tended to increase regardless of GCM, emission scenario, or time period.

4. Discussion

Forest carbon stock projections varied significantly as a function of treatment intensity within GCM and emission scenarios. Examining responses across GCMs and emission scenarios there was substantial variability in response to projected climate. The large influence of GCM on carbon storage suggests that reducing uncertainty in modeling forest growth response to wildfire mitigation treatments will require further refinement of climate projections. However, our results also suggest that there may be some capacity to leverage treatments to improve adaptive capacity for forest C sequestration as evidenced by the scenarios where there was little difference between control and thin-only treatments by the end of the simulation period (e.g. mid-century CNRM-A2). Our results show that changes in species-specific carbon stocks varied by GCM and emission scenario and that trade-offs between species caused a smaller reduction in stand-scale forest carbon stocks than would have occurred had all species been similarly impacted. The primary compensatory effects were between white fir and ponderosa pine, with late-century decreases in ponderosa pine carbon stocks being countered by increases in white fir carbon stocks for the GFDL and PCM1 GCMs under the A2 emission scenario. Some interesting compensatory dynamics also occurred with other species. For example, mid-century live tree carbon stocks showed small increases relative to the baseline control for CCSM3-B1 (Fig. 6). Under this scenario, white fir and sugar pine increased, while the other three species had slight decreases (Table 1).

Our results indicate that species-specific growth sensitivity to climate and the resultant carbon stock changes vary considerably as a function of the climate projections for a given emission scenario. Temperature increases throughout the century for all GCM-emission scenario combinations, with the greatest increase occurring with CCSM3 and the least with PCM1 (Figs. 2 and 3). Winter precipitation is quite variable among GCMs, but spring precipitation shows a decreasing trend for all GCMs (Fig. 2 and 3). Mid-century results show minimal effects of climate on the live tree carbon stock under both emission scenarios for CCSM3 and GFDL (Figs. 5 and 6). For this same period, the CNRM climate projection resulted in little change in carbon stocks from baseline for the B1 emission scenario; yet under the A2 scenario there was the largest percentage increase in live tree carbon relative to the baseline scenario (Fig. 6). This difference under the mid-century CNRM-A2 scenario may be due to substantial winter precipitation during the initial part of the simulation period, followed by a large increase over the last decade (Fig. 2). Over the first two decades of the CNRM-A2 mid-century simulation period, mean winter decadal precipitation was considerably higher than the other projections, but decreased by approximately 650 mm, before increasing by approximately 300 mm over the final decade of the simulation period (Fig. 2). Previous research has found that trees growing in a less competitive environment respond more quickly to changes in climate (Hurteau et al., 2007). This may provide some insight into the thin-only carbon stock attaining nearly the same level as the control over the length of the simulation period (Fig. 5).

Previous research on tree growth response to climate in the Sierra Nevada found minor change in precipitation coupled with increasing summer temperature could expedite the on-set of drought stress in this Mediterranean system, leading to a water-deficit induced reduction in growing season length (Battles et al., 2008). Battles et al. (2008) reported a decline in volume growth for trees grouped by "pines" and "firs and cedar", using downscaled climate projections from two GCMs (GFDL and PCM) under the same two emission scenarios (B1 and A2). By mid-century, we found slight overall declines in live tree carbon for both GFDL emission scenarios and PCM1-A2 (Fig. 6). Yet, under the mid-century PCM-B1 scenario, all species showed increases in live tree carbon, relative to baseline for all treatments. This pattern was especially pronounced for the burn-only and thin and burn treatments (Fig. 6). Winter precipitation and winter-spring precipitation were important factors controlling diameter growth for ponderosa pine

Table 1
Mean difference (calculated as projection minus baseline) in carbon stock from the baseline simulation for each GCM-treatment-species combination for mid-century (2020–2049) low (B1) and high (A2) emission scenarios. Standard errors are presented in parenthesis. The species are white fir (ABCO), red fir (ABMA), incense cedar (CADE), sugar pine (PILA), and ponderosa pine (PIPO). The GCM climate projections are from the National Center for Atmospheric Research Community Climate System Model (CCSM3), the Centre National de Recherches Météorologiques Coupled global Climate Model (CNRM CM3), the Geophysical Fluid Dynamics Lab coupled model (GFDL CM2.1), and the National Center for Atmospheric Research Parallel Climate Model (PCM1).

	CCSM3				CNRM				GFDL				PCM1			
	Control	Burn	Thin	Thin/Burn	Control	Burn	Thin	Thin/Burn	Control	Burn	Thin	Thin/Burn	Control	Burn	Thin	Thin/Burn
B1																
ABCO	2.31 (0.76)	2.09 (0.54)	2.75 (0.52)	1.62 (0.38)	−0.59 (1.54)	1.60 (0.75)	2.57 (0.78)	1.43 (0.61)	−5.79 (1.30)	−7.55 (1.43)	−7.37 (1.27)	−6.43 (1.15)	0.16 (1.09)	2.48 (0.89)	2.24 (0.77)	2.21 (0.70)
ABMA	−0.53 (0.45)	−0.51 (0.37)	−0.37 (0.20)	−0.17 (0.09)	−0.13 (0.44)	−0.39 (0.36)	−0.28 (0.16)	−0.04 (0.12)	0.38 (0.77)	−0.24 (0.18)	−0.19 (0.08)	−0.25 (0.20)	0.18 (0.39)	−0.26 (0.46)	−0.07 (0.16)	−0.06 (0.18)
CADE	−0.14 (0.19)	−0.16 (0.10)	−0.22 (0.15)	−0.15 (0.09)	−0.16 (0.21)	−0.10 (0.05)	−0.23 (0.19)	−0.07 (0.04)	−0.03 (0.32)	−0.14 (0.15)	−0.07 (0.15)	−0.11 (0.14)	0.63 (0.40)	0.33 (0.16)	−0.03 (0.16)	0.30 (0.15)
PILA	0.62 (0.44)	1.11 (0.53)	1.35 (0.77)	1.21 (0.58)	−0.05 (1.01)	0.87 (0.45)	0.02 (0.70)	0.81 (0.44)	1.41 (1.11)	0.46 (0.29)	0.47 (0.35)	0.37 (0.17)	0.71 (0.46)	0.72 (0.34)	0.94 (0.61)	0.88 (0.40)
PIPO	−1.32 (0.93)	−0.22 (0.70)	−0.17 (0.68)	−0.15 (0.69)	−0.90 (1.12)	−0.45 (0.40)	−0.98 (0.70)	−0.55 (0.34)	3.60 (1.49)	3.13 (1.49)	4.04 (1.59)	1.97 (1.36)	2.28 (1.47)	3.25 (1.36)	3.21 (1.46)	3.75 (1.35)
A2																
ABCO	−2.05 (1.11)	−4.40 (0.73)	−3.68 (0.59)	−4.00 (0.61)	4.43 (2.10)	8.58 (2.08)	8.99 (1.92)	7.82 (1.70)	−3.17 (0.96)	−4.51 (0.74)	−4.38 (0.73)	−4.26 (0.62)	−3.67 (1.51)	−5.03 (0.86)	−4.46 (0.50)	−4.77 (0.71)
ABMA	0.01 (0.63)	−0.42 (0.27)	−0.27 (0.17)	−0.20 (0.09)	0.14 (0.56)	−0.22 (0.16)	−0.15 (0.19)	0.01 (0.10)	0.35 (0.55)	−0.46 (0.34)	−0.27 (0.17)	−0.35 (0.12)	0.32 (0.56)	−0.66 (0.67)	−0.35 (0.33)	−0.11 (0.10)
CADE	0.02 (0.19)	−0.03 (0.06)	0.02 (0.07)	−0.02 (0.06)	0.05 (0.36)	0.26 (0.14)	−0.03 (0.63)	0.27 (0.14)	−0.25 (0.11)	−0.23 (0.07)	−0.74 (0.07)	−0.22 (0.06)	0.06 (0.33)	−0.09 (0.11)	−0.26 (0.11)	−0.10 (0.11)
PILA	0.54 (0.25)	0.74 (0.38)	1.38 (0.79)	0.75 (0.38)	0.85 (0.81)	1.40 (0.67)	1.03 (1.24)	1.48 (0.78)	0.08 (0.52)	0.53 (0.26)	0.86 (0.58)	0.47 (0.29)	0.15 (0.64)	0.42 (0.22)	0.49 (0.22)	0.38 (0.17)
PIPO	0.34 (0.86)	1.15 (0.55)	1.31 (0.74)	0.78 (0.44)	10.49 (2.44)	10.49 (1.67)	9.52 (1.90)	10.44 (1.66)	−1.87 (1.22)	−2.02 (1.00)	−2.08 (1.11)	−2.55 (0.92)	−2.60 (1.39)	−1.65 (0.62)	−2.17 (1.13)	−1.88 (0.55)

and white fir, respectively (Supplementary Tables S2 and S8). While there was a general decline in winter precipitation under the CNRM-A2 climate projection, it was greater than the other GCM projections for the first decade of the mid-century simulation period on both the east and west sides of the Basin (Fig. 2), likely contributing to the increase in carbon stocks relative to baseline for both species (Table 1). However, by late-century, this GCM projection resulted in small live tree carbon declines relative to baseline for both species (Table 2). Analysis of annual increment data from tree rings showed that ponderosa pine exhibited increased growth with warmer maximum winter and warmer minimum summer temperature (Robards, 2009). White fir exhibited a similar response to maximum winter temperature, but a negative growth relationship with increasing spring temperature (Robards, 2009). Since the FVS growth-and-yield model structure accounts for the effects of competition on growth (Crookston and Dixon, 2005) and previous research has shown that white fir is more responsive to changes in precipitation availability (Hurteau et al., 2007), the late-century increase in white fir for the CCSM3-A2 scenario may be a result of substantial increase in winter precipitation during the early part of the simulation period.

As identified by the recursive partitioning analysis, GCM was the most influential non-management factor affecting growth. This between GCM-emission scenario variability and the resultant growth response yielded substantial differences in live tree carbon stock, relative to the baseline (Fig. 6). However, under most climate projections from a specific GCM the relative differences between treatments remained similar to the baseline simulations for the first three time-steps of each simulation period. Under scenarios that live tree C stocks increased relative to baseline, treatments generally increased C stocks at a higher relative rate than did the control. Interestingly, only under the CNRM-A2 scenario did the thin-only live tree C approximate the control C by the end of the mid-century simulation period (Fig. 5). This was surprising given the common observation of tree growth-release following forest thinning (Latham and Tappeiner, 2002; McDowell et al., 2006; Fajardo et al., 2007). The growth-and-yield model, FVS, is the principal tool used by many forest managers to project forest growth because it effectively captures stand-level growth response to forest management practices, such as density reduction from fuels treatments. In FVS, tree growth following density reduction is most affected by the increase in resources, moderated by site productivity, resulting from reduced competition. Our results suggest that stand dynamics following treatment are sensitive to projected climate. While changing climate may alter how effectively different species can capture additional resources released by density reduction treatments, improving projections of the effect size of treatment under changing climate will require additional data from forest stands with a range of densities that have experienced climate variability over an extended period. Furthermore, our findings highlight the need to overcome the scale mismatch between GCMs and the typical forest management unit. Recent research suggests the substantial influence of local terrain on mediating climate (Dobrowski, 2011) making even downscaled climate projections too coarse to capture the fine scale climate variability that can influence tree growth. Our results also indicate that given the variability in climate projections among models, species-level modeling using only one or two climate projections is unlikely to capture much of the uncertainty due to the combination of this variability and the problems of model scale.

The results of this research must be considered in the context of the uncertainty of this approach. Linear mixed-effects models that include climate and topographic parameters were developed for annual diameter and height growth for each species (for specific details see Robards 2009). Robards (2009) reported that with the exception of red fir, AIC and REML metrics were minimized in

Table 2
Mean difference (calculated as projection minus baseline) in carbon stock from the baseline simulation for each GCM-treatment-species combination for late-century (2070–2099) low (B1) and high (A2) emission scenarios. Standard errors are presented in parenthesis. The species are white fir (ABCO), red fir (ABMA), incense cedar (CADE), sugar pine (PILA), and ponderosa pine (PIPO). The GCM climate projections are from the National Center for Atmospheric Research Community Climate System Model (CCSM3), the Centre National de Recherches Météorologiques Coupled global Climate Model (CNRM CM3), the Geophysical Fluid Dynamics Lab coupled model (GFDL CM2.1), and the National Center for Atmospheric Research Parallel Climate Model (PCM1).

	CCSM3				CNRM				GFDL				PCM1			
	Control	Burn	Thin	Thin/Burn	Control	Burn	Thin	Thin/Burn	Control	Burn	Thin	Thin/Burn	Control	Burn	Thin	Thin/Burn
B1																
ABCO	1.30 (1.05)	1.04 (0.53)	1.85 (0.58)	0.89 (0.39)	−0.02 (1.89)	3.12 (0.72)	3.26 (0.87)	2.64 (0.5)	−2.49 (1.24)	−3.76 (0.96)	−3.40 (0.85)	−4.03 (0.76)	−2.22 (1.07)	−1.55 (0.55)	−2.28 (0.84)	−1.57 (0.57)
ABMA	−0.69 (0.74)	−0.78 (0.51)	−0.76 (0.65)	−0.41 (0.25)	0.25 (0.72)	−0.12 (0.15)	0.10 (0.24)	0.07 (0.05)	0.23 (0.69)	−0.50 (0.27)	−0.47 (0.32)	−0.24 (0.11)	0.09 (0.39)	−0.71 (0.30)	−0.47 (0.49)	−0.47 (0.35)
CADE	−0.10 (0.23)	−0.08 (0.44)	−0.35 (0.06)	−0.05 (0.04)	−0.02 (0.29)	0.10 (0.29)	−0.13 (0.09)	0.10 (0.08)	−0.34 (0.36)	−0.37 (0.36)	−0.56 (0.18)	−0.35 (0.17)	−0.07 (0.13)	−0.23 (0.13)	−0.10 (0.10)	−0.20 (0.10)
PI LA	1.50 (0.90)	1.61 (0.70)	1.43 (0.81)	1.71 (0.88)	0.03 (0.59)	0.93 (0.40)	0.50 (0.48)	1.02 (0.51)	0.96 (0.61)	0.61 (0.63)	1.02 (0.40)	0.56 (0.29)	0.59 (0.73)	−0.10 (0.24)	0.18 (0.15)	0.08 (0.15)
PIPO	2.15 (1.08)	2.29 (0.75)	2.59 (0.80)	2.11 (0.74)	7.88 (1.68)	7.70 (1.49)	7.68 (1.28)	6.96 (1.21)	−5.84 (1.53)	−5.74 (1.48)	−5.96 (1.30)	−5.79 (1.35)	−4.77 (1.28)	−4.68 (1.15)	−5.01 (0.93)	−4.32 (0.85)
A2																
ABCO	5.48 (1.23)	5.67 (1.15)	6.28 (0.99)	4.84 (0.82)	−2.35 (0.96)	−1.63 (0.38)	−0.73 (0.66)	−2.00 (0.57)	7.22 (1.37)	6.41 (1.29)	7.24 (1.39)	6.07 (1.35)	0.34 (0.68)	1.17 (0.51)	1.16 (0.47)	0.52 (0.40)
ABMA	−0.93 (0.42)	−0.84 (0.39)	−0.64 (0.59)	−0.18 (0.11)	0.14 (0.28)	−0.78 (0.38)	−0.60 (0.46)	−0.39 (0.31)	−0.82 (0.82)	−0.46 (0.30)	−0.48 (0.34)	−0.37 (0.13)	0.21 (0.16)	−0.46 (0.35)	−0.31 (0.60)	−0.30 (0.31)
CADE	−0.37 (0.27)	−0.15 (0.20)	−0.03 (0.08)	−0.11 (0.08)	−0.27 (0.18)	−0.22 (0.18)	0.01 (0.10)	−0.18 (0.09)	−0.88 (0.23)	−0.36 (0.23)	−0.45 (0.14)	−0.36 (0.15)	0.15 (0.22)	−0.08 (0.22)	−0.21 (0.09)	−0.07 (0.09)
PI LA	0.14 (1.05)	1.28 (1.00)	1.95 (0.66)	1.51 (0.77)	1.05 (0.85)	1.03 (1.19)	−0.13 (0.49)	0.96 (0.51)	1.27 (0.56)	0.76 (0.54)	0.89 (0.40)	0.96 (0.60)	0.79 (0.29)	0.81 (0.42)	0.59 (0.38)	0.90 (0.43)
PIPO	−1.14 (1.07)	−0.14 (0.97)	−0.56 (0.79)	0.22 (0.79)	−1.13 (1.45)	−0.08 (1.04)	−1.86 (0.8)	−1.08 (0.80)	−5.72 (1.58)	−3.97 (1.41)	−4.29 (1.37)	−3.87 (1.26)	−2.57 (0.86)	−2.34 (0.76)	−2.04 (0.64)	−2.20 (0.68)

the final models. In the case of red fir the inclusion of latitude as a model parameter resulted in a less parsimonious model, however latitude was retained in the final model to account for the latitudinal gradient that is present in this species' distribution. While this approach facilitates the inclusion of climatic and topographic information, parameters which are typically absent from growth-and-yield models, the models are empirically-based and may be incapable of predicting growth response to conditions outside the range used for their development, including extreme climatic events such as prolonged, acute drought-stress. Additionally, the uncertainty associated with downscaling global scale climate projections is inherent in this approach. As noted by Cayan et al. (2008), the complex topography in California and the effects of increasing temperature on Sierran snowpack require regional models to distribute climate. The approach taken here considers only the impacts of physical climate drivers on tree species' growth. The increased atmospheric CO_2 that underlies the altered climatic variables increases NPP in short-term experimental studies of young forest stands (Norby et al., 2010), yet progressive nitrogen limitation (Luo et al., 2004; Reich et al., 2006) may strongly constrain longer-term ecosystem response to CO_2. Because of increased water use efficiency, CO_2 might mitigate productivity reductions in drier future conditions. Whether this would alter species-level responses depends in part on variation in these conifer species' photosynthetic and water use efficiency responses to elevated CO_2, something that is not currently known. Further, because we did not alter the mortality function in the model we were unable to capture potential climate-driven transitions of C from the live tree to the dead tree C pool. Previous research has shown that tree mortality has the potential to increase with increasing drought stress (van Mantgem et al., 2009; Williams et al., 2012; Loudermilk et al., 2013) and increasing mortality could influence the carbon dynamics.

Another factor not addressed by this study is the projected effect of climate on wildfire and the combined influences of climate and wildfire on forest carbon stocks. The frequency of large wildfires is projected to increase in California with changing climate (Westerling and Bryant, 2008). Research on climate-driven changes in fire regimes in Washington indicates that the effects of increasing area burned by wildfire could result in sizable reduction in forest carbon stocks (Raymond and McKenzie, 2012). While under historical and current climatic conditions land-use and disturbance have been the primary regional factors influencing carbon storage relative to the theoretical maximum (Smithwick et al., 2002; Hudiburg et al., 2009), the effects of changing climate on forest growth are likely to exert a significant influence on the carbon carrying capacity of the system. In the context of this research, the results of the recursive partitioning analysis identified GCM as the most important factor controlling forest carbon stocks. Had our study included increasing wildfire probability, the effects of management treatments may have been more pronounced because of the influence of these treatments on changing fire behavior and tree mortality rates (Stephens and Moghaddas, 2005). However, our results do indicate that under several of the projected climate scenarios (e.g. CNRM-B1, GFDL-B1, and PCM1-A2) the results of the simulated management actions suggest no interaction between climate and management (Fig. 6). Understanding interactions among climate, wildfire frequency, and forest growth deserves further research.

Informed estimates of the impacts of changing climatic conditions on forest growth are of great importance to carbon offset project development. To have value, forest carbon offset projects must sequester more carbon than business-as-usual (additionality) and maintain the carbon stock for some required period of time (permanence). Forest carbon accounting protocols, such as the one used by the Climate Action Reserve (2010), require baseline

projections of the business-as-usual condition against which additionality is quantified. The majority of the growth-and-yield models do not account for the effects of changing climate on forest growth, potentially leading to an incorrect estimate of the future baseline condition. Incorrect baseline estimates detract from the economic viability of a project if carbon stock difference between the baseline condition and the project is reduced to the point that the project value is insufficient to cover the cost of investment.

The results of this study highlight the complexity of modeling how different species will be affected by stand-level dynamics under changing climatic conditions. Modeled climate projections for California suggest late-century mean temperature increases ranging from 1.5 to 4.5 °C, relatively small changes in precipitation, and reduced snowpack with increased warming (Cayan et al., 2008). As our results and the results of Battles et al. (2008) indicate, the potential exists for a weakening of the carbon sink strength in these mixed-conifer forests. The strength of this positive biogeochemical feedback to warming may be enhanced by increased wildfire frequency (Westerling and Bryant, 2008) and climatically driven mortality (vanMantgem et al., 2009). Forest structural manipulations, such as thinning and prescribed burning, can reduce water, nutrient, and light competition and the risk of stand-replacing fire (Kaye et al., 2005; McDowell et al., 2006; Stephens et al., 2009a). However, the current variability in downscaled global climate projections adds considerable uncertainty to projecting how management actions to alter forest structure and composition and climate will interact in the future. Additional investigation into the effects of climate on regeneration and mortality is needed. Better characterization of these processes will help improve projections of stand dynamics under changing climate. Given the variation in species-specific carbon stocks in response to the range of emission and climate scenarios used to drive these simulations, our results suggest that an equitable distribution of basal area between species may provide the best hedge against this uncertainty.

Acknowledgements

This research was supported by Cooperative Agreement 08-CA-11272170-102 with the US Department of Agriculture Forest Service Pacific Southwest Research Station, using funds provided by the Bureau of Land Management through the sale of public lands authorized by the Southern Nevada Public Land Management Act. We thank Sarah Robards-Sheaks, Research Assistant with Spatial Informatics Group, LLC, for providing technical support for the simulations. We also thank Jeff Hicke and two anonymous reviewers for providing constructive feedback on a previous version of this manuscript.

Appendix A. Supplementary material

Supplementary data associated with this article can be found, in the online version, at http://dx.doi.org/10.1016/j.foreco.2013.12.012.

References

Battles, J.J., Robards, T., Das, A., Waring, K., Gilles, J.K., Biging, G., Schurr, F., 2008. Climate change impacts on forest growth and tree mortality: a data-driven modeling study in the mixed-conifer forest of the Sierra Nevada, California. Clim. Change 87 (Suppl. 1), S193–S213.
Beaty, R.M., Taylor, A.H., 2008. Fire history and the structure and dynamics of a mixed conifer forest landscape in the northern Sierra Nevada, Lake Tahoe Basin, California, USA. For. Ecol. Manage. 255, 707–719.
Breiman, L., Friedman, J., Stone, C.J., Olshen, R.A., 1984. Classification and Regression Trees. Chapman & Hall/CRC, Boca Raton, FL.
Brown, J.K., 1974. Handbook for inventorying downed woody material. US Department of Agriculture, Forest Service, Intermountain Forest and Range Experiment Station, Gen. Tech. Rep. INT-16 Ogden, UT.
Campbell, J.L., Harmon, M.E., Mitchell, S.R., 2012. Can fuel-reduction treatments really increase forest carbon storage in the western US by reducing future fire emissions? Front. Ecol. Environ. 10, 83–90.
Canadell, J.G., Raupach, M.R., 2008. Managing forests for climate change mitigation. Science 320, 1456.
Cayan, D., Tyree, M., Dettinger, M.D., Hidalgo, H.G., Das, T., Maurer, E.P., Bromirski, P., Graham, N., Flick, R., 2009. In: Center, C.C.C. (Ed.), Climate Change Scenarios and Sea Level Rise Estimates for the California 2009 Climate Change Scenarios Assessment, p. 50.
Cayan, D.R., Maurer, E.P., Dettinger, M.D., Tyree, M., Hayhoe, K., 2008. Climate change scenarios for the California region. Clim. Change 87 (Suppl. 1), S21–S42.
ClimateActionReserve, 2010. Forest Project Protocol v3.2.
Crookston, N.L., Dixon, G.E., 2005. The forest vegetation simulator: a review of its structure, content, and applications. Comput. Electron. Agric. 49, 60–80.
Crookston, N.L., Rehfeldt, G.E., Dixon, G.E., Weiskittel, A.R., 2010. Addressing climate change in the forest vegetation simulator to assess impacts on landscape forest dynamics. For. Ecol. Manage. 260, 1198–1211.
Dickson, B.G., Prather, J.W., Xu, Y., Hampton, H.M., Aumack, E.N., Sisk, T.D., 2006. Mapping the probability of large fire occurrence in northern Arizona, USA. Landscape Ecol. 21, 747–761.
Dobrowski, S.Z., 2011. A climatic basis for microrefugia: the influence of terrain on climate. Glob. Change Biol. 17, 1022–1035.
Dore, S., Kolb, T.E., Montes-Helu, M., Sullivan, B.W., Winslow, W.D., Hart, S.C., Kaye, J.P., Koch, G.W., Hungate, B.A., 2008. Long-term impact of a stand-replacing fire on ecosystem CO_2 exchange of a ponderosa pine forest. Glob. Change Biol. 14, 1–20.
Eliott-Fisk, D.L., Cahill, T.C., Davis, O.K., Duan, L., Goldman, C.R., Gruell, G.E., Harris, R., Kattlemann, R., Lacey, R., Leisz, D., Lindstrom, S., Machida, D., Rowntree, R.A., Rucks, P., Sharkey, D.A., Stephens, S.L., Ziegler, D.S., 1996. Lake Tahoe Case Study. Sierra Nevada Ecosystem Project: Final Report to Congress. Addendum I. University of California Centers for Wildland Resources, Davis, CA, pp. 217–276.
Everitt, B.S., Hothorn, T., 2006. A Handbook of Statistical Analyses using Rpart. Chapman & Hall/CRC, Boca Raton, FL.
Fajardo, A., Graham, J.M., Goodburn, J.M., Fiedler, C.E., 2007. Ten-year responses of ponderosa pine growth, vigor, and recruitment to restoration treatments in the Bitteroot Mountains, Montana, USA. For. Ecol. Manage. 243, 50–60.
FIA, 2009a. Regional Biomass Equations used by FIA to Estimate Bole, Bark and Branches. USDA Forest Service, Pacific Northwest Research Station.
FIA, 2009b. Volume Estimation for the PNW-FIA Integrated Database. USDA Forest Service, Pacific Northwest Research Station.
Flannigan, M.D., Stocks, B.J., Wotton, B.M., 2000. Climate change and forest fires. Sci. Total Environ. 262, 221–229.
Galik, C.S., Jackson, R.B., 2009. Risks to forest carbon offset projects in a changing climate. For. Ecol. Manage. 257, 2209–2216.
Gullison, R.E., Frumhoff, P.C., Canadell, J.G., Field, C.B., Nepstad, D.G., Hayhoe, K., Avissar, R., Curran, L.M., Friedlingstein, P., Jones, C.D., Nobre, C., 2007. Tropical forests and climate policy. Science 316, 985–986.
Harlow, W.M., Harrar, E.S., Hardin, J.W., White, F.M., 1996. Textbook of Dendrology. McGraw-Hill Inc., New York.
Hidalgo, H.G., Dettinger, M.D., Cayan, D.R., 2008. Downscaling with Constructed Analogues: Daily Precipitation and Temperature Fields over the United States. California Energy Commission. Report CEC-500-2007-123.
Hudiburg, T., Law, B., Turner, D.P., Campbell, J., Donato, D., Duane, M., 2009. Carbon dynamics of Oregon and Northern California forests and potential land-based carbon storage. Ecol. Appl. 19, 163–180.
Hurteau, M., Zald, H., North, M., 2007. Species-specific response to climate reconstruction in upper-elevation mixed-conifer forests of the western Sierra Nevada, California. Can. J. For. Res. 37, 1681–1691.
Hurteau, M.D., Brooks, M.L., 2011. Short- and long-term effects of fire on carbon in US dry temperate forest systems. Bioscience 61, 139–146.
Hurteau, M.D., Hungate, B.A., Koch, G.W., 2009. Accounting for risk in valuing forest carbon offsets. Carbon Balance Manage. 4, 1.
Hurteau, M.D., Hungate, B.A., Koch, G.W., North, M.P., Smith, G.R., 2013. Aligning ecology and markets in the forest carbon cycle. Front. Ecol. Environ. 11, 37–42.
Hurteau, M.D., Stoddard, M.T., Fule, P.Z., 2011. The carbon costs of mitigating high-severity wildfire in southwestern ponderosa pine. Glob. Change Biol. 17, 1516–1521.
Kaye, J.P., Hart, S.C., Fule, P.Z., Covington, W.W., Moore, M.M., Kaye, M.W., 2005. Initial carbon, nitrogen, and phosphorous fluxes following ponderosa pine restoration treatments. Ecol. Appl. 15, 1581–1593.
Keith, H., Mackey, B.G., Lindenmayer, D.B., 2009. Re-evaluation of forest biomass carbon stocks and lessons from the world's most carbon-dense forests. Proc. Nat. Acad. Sci. 106, 11635–11640.
Keyser, C.E., 2008. Western Sierra Nevada (WS) Variant Overview – Forest Vegetation Simulator. U.S. Department of Agriculture, Forest Service, Forest Management Service Center, Fort Collins, CO (revised July 29, 2010).
Latham, P., Tappeiner, J., 2002. Response of old-growth conifers to reduction in stand density in western Oregon forests. Tree Physiol. 22, 137–146.
Lenihan, J.M., Bachelet, D., Neilson, R.P., Drapek, R.J., 2008. Response of vegetation distribution, ecosystem productivity, and fire to climate change scenarios in California. Clim. Change 87 (Suppl. 1), S215–S230.
Lenihan, J.M., Drapek, R.J., Bachelet, D., Neilson, R.P., 2003. Climate change effects on vegetation distribution, carbon, and fire in California. Ecol. Appl. 13, 1667–1681.

Loudermilk, E.L., Scheller, R.M., Weisberg, P.J., Yang, J., Dilts, T.E., Karam, S.L., Skinner, C., 2013. Carbon dynamics in the future forest: the importance of long-term successional legacy and climate-fire interactions. Glob. Change Biol. 19, 3502–3515.
Luo, Y., Su, B., Currie, W.S., Dukes, J.S., Finzi, A., Hartwig, U., Hungate, B.A., McMurtrie, R.E., Oren, R., Parton, W.J., Pataki, D.E., Shaw, M.R., Zak, D.R., Field, C.B., 2004. Progressive nitrogen limitation of ecosystem responses to rising atmospheric carbon dioxide. Bioscience 54, 731–739.
Maurer, E.P., Hidalgo, H.G., 2008. Utility of daily vs. monthly large-scale climate data: an intercomparison of two statistical downscaling methods. Hydrol. Earth Syst. Sci. 12, 551–563.
McDowell, N.G., Adams, H.D., Bailey, J.D., Hess, M., Kolb, T.E., 2006. Homeostatic maintenance of ponderosa pine gas exchange in response to stand density changes. Ecol. Appl. 16, 1164–1182.
Mitchell, S.R., Harmon, M.E., O'Connell, K.E.B., 2009. Forest fuel reduction alters fire severity and long-term carbon storage in three Pacific Northwest ecosystems. Ecol. Appl. 19, 643–655.
Murthy, S.K., 1998. Automatic construction of decision trees from data: a multi-disciplinary survey. Data Min. Knowl. Disc. 2, 345–389.
Norby, R.J., Warren, J.M., Iversen, C.M., Medlyn, B.E., Mcurtrie, R.E., 2010. CO_2 enhancement of forest productivity constrained by limited nitrogen availability. Proc. Nat. Acad. Sci. 107, 19368–19373.
North, M., Hurteau, M., Fiegener, R., Barbour, M., 2005. Influence of fire and El Niño on tree recruitment varies by species in Sierran mixed conifer. For. Sci. 51, 187–197.
North, M., Hurteau, M., Innes, J., 2009. Fire suppression and fuels treatment effects on mixed-conifer carbon stocks and emissions. Ecol. Appl. 19, 1385–1396.
North, M., Innes, J., Zald, H., 2007. Comparison of thinning and prescribed fire restoration treatments to Sierran mixed-conifer historic conditions. Can. J. For. Res. 37, 331–342.
Pacala, S., Socolow, R., 2004. Stabilization wedges: solving the climate problem for the next 50 years with current technologies. Science 305, 968–972.
Pearson, R.G., Dawson, T.P., 2003. Predicting the impacts of climate change on the distribution of species: are bioclimate envelope models useful? Glob. Ecol. Biogeogr. 12, 361–371.
Pechony, O., Shindell, D.T., 2010. Driving forces of global wildfires over the past millennium and the forthcoming century. Proc. Nat. Acad. Sci. 107, 19167–19170.
Raymond, C.L., McKenzie, D., 2012. Carbon dynamics of forests in Washington, USA: 21st century projections based on climate-driven changes in fire regimes. Ecol. Appl. 22, 1589–1611.
Reich, P.B., Hungate, B.A., Luo, Y., 2006. Carbon-nitrogen interactions in terrestrial ecosystems in response to rising atmospheric carbon dioxide. Annu. Rev. Ecol. Evol. Syst. 37, 611–636.
Robards, T., 2009. Empirical Forest Growth Model Evaluations and Development of Climate-Sensitive Hybrid Models. University of California, Berkeley, Berkeley, p. 234.
Seager, R., Ting, M., Held, I., Kushnir, Y., Lu, J., Vecchi, G., Huang, H.-P., Hamik, N., Leetmaa, A., Lau, N.-C., Li, C., Velez, J., Naik, N., 2007. Model projections of an imminent transition to a more arid climate in southwestern North America. Science 316, 1181–1184.
Smithwick, E.A.H., Harmon, M.E., Remillard, S.M., Acker, S.A., Franklin, J.F., 2002. Potential upper bounds of carbon stores in forests of the Pacific Northwest. Ecol. Appl. 12, 1303–1317.
Stephens, S.L., Moghaddas, J.J., 2005. Experimental fuel treatment impacts on forest structure, potential fire behavior, and predicted tree mortality in a California mixed conifer forest. For. Ecol. Manage. 215, 21–36.
Stephens, S.L., Moghaddas, J.J., Edminster, C., Fiedler, C.E., Haase, S., Harrington, M., Keeley, J.E., Knapp, E.E., McIver, J.D., Metlen, K., Skinner, C.N., Youngblood, A., 2009a. Fire treatment effects on vegetation structure, fuels, and potential fire severity in western U.S. forests. Ecol. Appl. 19, 305–320.
Stephens, S.L., Moghaddas, J.J., Hartsough, B.R., Moghaddas, E.E.Y., Clinton, N.E., 2009b. Fuel treatment effects on stand-level carbon pools, treatment-related emissions, and fire risk in a Sierra Nevada mixed-conifer forest. Can. J. For. Res. 39, 1538–1547.
Therneau, T.M., Atkinson, B., Ripley, B., 2007. The Rpart Package.
van Mantgem, P.J., Stephenson, N.L., Byrne, J.C., Daniels, L.D., Franklin, J.F., Fule, P.Z., Harmon, M.E., Larson, A.J., Smith, J.M., Taylor, A.H., Veblen, T.T., 2009. Widespread increase of tree mortality rates in the western United States. Science 323, 521–524.
VandeWater, K., North, M., 2010. Fire history of coniferous riparian forests in the Sierra Nevada. For. Ecol. Manage. 260, 384–395.
vanMantgem, P.J., Stephenson, N.L., Byrne, J.C., Daniels, L.D., Franklin, J.F., Fule, P.Z., Harmon, M.E., Larson, A.J., Smith, J.M., Taylor, A.H., Veblen, T.T., 2009. Widespread increase of tree mortality rates in the western United States. Science 323, 521–524.
West, B.T., Welch, K.B., Galecki, A.T., 2007. Linear Mixed Models: A Practical Guide using Statistical Software. Chapman & Hall/CRC, Boca Raton, FL.
Westerling, A.L., Bryant, B.P., 2008. Climate change and wildfire in California. Clim. Change 87 (Suppl. 1), S231–S249.
Westerling, A.L., Turner, M.G., Smithwick, E.A.H., Romme, W.H., Ryan, M.G., 2011. Continued warming could transform greater Yellowstone fire regimes by mid-21st century. Proc. Nat. Acad. Sci. 108, 13165–13170.
Williams, A.P., Allen, C.D., Macalady, A.K., Griffin, D., Woodhouse, C.A., Meko, D.M., Swetnam, T.W., Rauscher, S.A., Seager, R., Grissino-Mayer, H.D., Dean, J.S., Cook, E.R., Gangodagamage, C., Cai, M., McDowell, N.G., 2012. Temperature as a potent driver of regional forest drought stress and tree mortality. Nat. Clim. Change 3, 292–297.
Winford, E.M., Gaither Jr., J.C., 2012. Carbon outcomes from fuels treatment and bioenergy production in a Sierra Nevada forest. For. Ecol. Manage. 282, 1–9.
Zald, H.S.J., Gray, A.N., North, M., Kern, R.A., 2008. Initial tree regeneration responses to fire and thinning treatments in a Sierra Nevada mixed-conifer forest, USA. For. Ecol. Manage. 256, 168–179.

Supplementary Information

Tree growth increment data sources used for developing species-specific growth relationships included growth data from four data sets representing sites throughout northern California (Table S1). The data sets included:

NCStem: Stem analysis data from the Northern California Forest Yield Cooperative (Biging 1983).
NCPlot: Permanent plot and increment core data from the Northern California Forest Yield Cooperative (Wensel 1987).
DolphMC: Mixed conifer increment core and permanent plot data from the USDA Forest Service, Pacific Southwest Research Station (Dolph 1988, Dolph and Amidon 1979).
DolphRF: Red fir data from the USDA Forest Service, Pacific Southwest Research Station (Dolph 1992).
Table S1: Data used for model fitting of individual tree growth equations.

Data Source	**Years Covered**	**No. of Plots**	**No. of Trees**	**No. of Diameter Increments**	**No. of Height Increments**
NCStem	1965-1980	105	5465	4639	2436
NCPlot	1961-1998	622	31807	3725	2991
DolphMC	1958-1988	397	3232	4436	1417
DolphRF	1964-1987	254	1955	3564	1296

A linear mixed effects model was used for both diameter and height growth. Confidence intervals were estimated using 1000 observations from Markov Chain Monte Carlo (MCMC) simulation. Final model structure for each species was selected using the Akaike Information Criterion (AIC) and Residual Maximum Likelihood Estimation (REML) to evaluate explanatory power and parsimony are presented in Tables S2-S11. With the exception of AIC for sugar pine and both measures for red fir, AIC and REML were minimized for the final models. The addition of the variable latitude was significant (α=0.05) for red fir. However, the model penalty was accepted to retain this variable within the structure. Individual parameters were evaluated by examining the confidence intervals from the MCMC simulations using a 95% confidence level applied to the Student's t-value (Tables S12-S21). The parameter abbreviations are as follows:

DBH: diameter at breast height
CR: crown ratio
PBAL: plot level basal area
THT: Total height
PRECIP_XXX: Total precipitation in a given season
MAXT5DAYS_XXX: Number of days with mean daily maximum temperature above 5°C for a given season
MAXT10DAYS_XXX: Number of days with mean daily maximum temperature above 10°C for a given season
MINT5DAYS_XXX: Number of days with mean daily minimum temperature above 5°C for a given season

MINT10DAYS_XXX: Number of days with mean daily minimum temperature above 10°C for a given season
ELEV: elevation
ASP: aspect

Table S2: Parameter attributes for the ponderosa pine diameter growth model.

Variable	**Minimum**	**Median**	**Mean**	**Maximum**
Diameter Growth (in)	0.0040	0.1301	0.1495	1.3650
DBH (in)	6.01	14.00	15.05	69.37
CR	0.042	0.509	0.518	1.000
PBAL	0.00	61.15	78.13	595.70
PRECIP_WIN (mm x 10)	1712	7498	7740	19610
MAXT10DAYS_WIN (days) [% of season days]	17 [11]	72 [48]	75.18 [50]	151 [100]
MAXT5DAYS_SPR (days) [% of season days]	37 [40]	92 [100]	90.18 [98]	92 [100]
MAXT5DAYS_SUM(days) [% of season days]	0 [0]	121 [99]	114.1 [94]	122 [100]
SLOPE (%)	0	15	17.91	70
ASP (deg)	0	180	181.3	360
ELEV (ft)	2650	4320	4293	9000
UTMY-W (west)	4379	4541	4519	4648
UTMY-E (east	3993	4421	4399	4747

Table S3: Parameter attributes for the ponderosa pine height growth model.

Variable	**Minimum**	**Median**	**Mean**	**Maximum**
Height Growth (ft)	0.060	0.914	1.035	4.998
THT (ft)	11.00	73.00	73.54	184
CR	0.035	0.511	0.519	1.000
PBAL	0.00	66.68	83.31	641.20
PRECIP_WIN (mm x 10)	1712	7571	7716	19610
PRECIP_SPRSUM (mm x 10)	380	3786	3695	7972
MAXT10DAYS_WIN (days) [% of season days]	17 [11]	70 [46]	73.28 [49]	151 [100]
MAXT5DAYS_SPR (days) [% of season days]	37 [40]	92 [100]	90.02 [98]	92 [100]
MAXT5DAYS_SUM(days) [% of season days]	0 [0]	122 [100]	119.7 [98]	122 [100]

SLOPE (%)	0	15	17.51	70
ASP (deg)	0	180	178.7	360
ELEV (ft)	2650	4240	4263	9000
UTMY-W (west)	4379	4569	4525	4648
UTMY-E (east	3993	4440	4419	4634

Table S4: Parameter attributes for the sugar pine diameter growth model.

Variable	**Minimum**	**Median**	**Mean**	**Maximum**
Diameter Growth (in)	0.0080	0.1998	0.2226	0.9651
DBH (in)	6.02	14.97	16.81	65.93
CR	0.033	0.559	0.532	1.000
PBAL	0.00	60.50	84.49	482.70
PRECIP_WIN (mm x 10)	1769	9186	9209	19610
MINT5DAYS_WIN (days) [% of season days]	0 [0]	6 [4]	9.677 [6]	53 [35]
MINT5DAYS_SPR (days) [% of season days]	0 [0]	6 [7]	11.55 [13]	64 [70]
MINT5DAYS_SUM(days) [% of season days]	0 [0]	118 [97]	109.9 [90]	122 [100]
SLOPE (%)	0	11	20	70
ASP (deg)	0	180	185	360
ELEV (ft)	2350	4680	4661	6602
UTMY	4108	4417	4394	4642

Table S5: Parameter attributes for the sugar pine height growth model.

Variable	**Minimum**	**Median**	**Mean**	**Maximum**
Height Growth (ft)	0.0500	1.020	1.122	4.496
THT (ft)	10	75	75.97	199
CR	0.033	0.529	0.537	0.952
PBAL	0.00	60.37	86.10	543.80
PRECIP_SPRSUM (mm x 10)	380	4374	4294	7972
MINT5DAYS_SPR (days) [% of season days]	0 [0]	6 [7]	12.32 [14]	64 [70]
MINT10DAYS_WIN (days) [% of season days]	0 [0]	0 [0]	0.244 [0]	16 [11]
SLOPE (%)	0	20	21.91	70
ASP (deg)	0	180	187.8	360
ELEV (ft)	2350	4680	4622	6602
UTMY-W (west)	4416	4518	4507	4635
UTMY-E (east	4120	4406	4382	4642

Table S6: Parameter attributes for incense-cedar diameter growth model.

Variable	Minimum	Median	Mean	Maximum
Diameter Growth (in)	0.0100	0.1232	0.1466	1.2590
DBH (in)	6.01	11.30	13.06	69.90
CR	0.036	0.552	0.547	0.978
PBAL	0.00	86.14	106.70	660.80
PRECIP_WIN (mm x 10)	1712	8138	8497	17510
PRECIP_SUM (mm x 10)	0	605	628.3	1389
MINT5DAYS_WIN (days) [% of season days]	0 [0]	10 [7]	11.4 [8]	43 [28]
MAXT5DAYS_SPR (days) [% of season days]	37 [40]	92 [100]	90.39 [98]	92 [100]
MAXT5DAYS_SUM(days) [% of season days]	0 [0]	122 [100]	119.6 [98]	122 [100]
SLOPE (%)	0	18	18.95	75
ASP (deg)	0	180	184.5	360
ELEV (ft)	2650	4545	4544	6640
UTMY-W (west)	4408	4569	4526	4659
UTMY-E (east)	4108	4302	4341	4720

Table S7: Parameter attributes for incense-cedar height growth model.

Variable	Minimum	Median	Mean	Maximum
Height Growth (ft)	0.0700	0.6252	0.7642	4.8700
THT (ft)	10	44	48.77	185
CR	0.034	0.564	0.559	1.000
PBAL	0.00	73.50	95.87	630.00
PRECIP_WIN (mm x 10)	1712	8472	8625	17510
MINT5DAYS_WIN (days) [% of season days]	0 [0]	11 [7]	11.42 [8]	43 [28]
MAXT5DAYS_SPR (days) [% of season days]	37 [40]	92 [100]	90.24 [98]	92 [100]
TMAX_SUM (deg C x 100)	1595	2595	2598	3449
SLOPE (%)	0	17	18.78	75
ASP (deg)	0	180	181.8	360
ELEV (ft)	2650	4550	4543	6640
UTMY	4108	4326	4364	4659

Table S8: Parameter attributes for white fir diameter growth model.

Variable	Minimum	Median	Mean	Maximum
Diameter Growth (in)	0.0068	0.1740	0.1915	1.5390
DBH (in)	6.01	12.10	13.50	80.71
CR	0.016	0.532	0.538	1.000
PBAL	0.00	73.52	95.89	630.00
PRECIP_WINSPR (mm x 10)	2613	12160	12260	26720
PRECIP_SUM (mm x 10)	214	696	703.3	1580
MAXT5DAYS_WIN (days) [% of season days]	37 [25]	139 [92]	132.6 [88]	151 [100]
MAXT5DAYS_SPR (days) [% of season days]	0 [0]	73 [79]	70.7 [77]	92 [100]
MAXT5DAYS_SUM(days) [% of season days]	100 [82]	122 [100]	120.3 [99]	122 [100]
SLOPE (%)	0	19	20.53	78
ASP (deg)	0	180	179.3	360
ELEV (ft)	2700	5000	5024	8000
UTMY-W (west)	4386	4574	4535	4659
UTMY-E (east)	3976	4409	4407	4747

Table S9: Parameter attributes for white fir height growth model.

Variable	Minimum	Median	Mean	Maximum
Height Growth (ft)	0.0100	0.9898	1.0780	4.878
THT (ft)	10.00	62.30	65.37	174.00
CR	0.031	0.548	0.554	1.000
PBAL	0.00	76.82	101.50	644.00
PRECIP_WIN (mm x 10)	1712	9030	8905	19610
MAXT5DAYS (days) [% of season days]	205 [56]	353 [97]	345.2 [95]	365 [100]
TMAX_WIN (deg C x 100)	401	1000	999	1699
TMAX_SPR (deg C x 100)	587	1394	1399	2370
TMAX_SUM (deg C x 100)	1595	2527	2519	3449
ELEV (ft)	2750	4900	4933	7900
UTMY-W (west)	4386	4574	4542	4659
UTMY-E (east)	3976	4423	442	4747

Table S10: Parameter attributes for red fir diameter growth model.

Variable	Minimum	Median	Mean	Maximum
Diameter Growth (in)	0.011	0.190	0.208	1.485
DBH (in)	6.01	13.56	14.88	69.98
CR	0.094	0.573	0.570	0.978
PBAL	0.00	47.57	62.82	440.20
PRECIP_WIN (mm x 10)	3371	8437	8729	23890
PRECIP_SUM (mm x 10)	137	778	768.1	2384
MAXT10DAYS_WIN (days) [% of season days]	23 [15]	37 [25]	41.44 [27]	117 [77]
MAXT5DAYS_SPR (days) [% of season days]	61 [66]	86 [93]	84.75 [92]	92 [100]
MAXT10DAYS_SUM(days) [% of season days]	106 [87]	122 [100]	121.6 [100]	122 [100]
SLOPE (%)	0	21	22.4	60
ASP (deg)	0	192	186.6	360
ELEV (ft)	2700	6500	6524	9000
UTMY	4301	4385	4415	1635

Table S11: Parameter attributes for red fir height growth model.

Variable	Minimum	Median	Mean	Maximum
Height Growth (ft)	0.040	1.001	1.052	4.871
THT (ft)	10	60	59.74	127
CR	0.091	0.571	0.573	0.978
PRECIP_SPR (mm x 10)	895	2992	3146	7714
MAXT10DAYS_WIN (days) [% of season days]	23 [15]	39 [26]	42.53 [28]	117 [77]
SLOPE (%)	0	21	22.62	60
ASP (deg)	0	160	174	360
ELEV (ft)	2700	6200	6274	9000
UTMY	3976	4472	4468	4747

The final model coefficients for each species-specific diameter and height growth model are presented in Tables S12-S21.

Table S12: Coefficients and statistics for ponderosa pine diameter growth model.

Parameter	Coefficient	Std Error	t-value	Lower 95% CI	Upper 95% CI
Intercept	-4.552	0.6341	-7.179	-5.3382	-2.7232
Log(DBH)	0.8938	0.07075	12.633	0.6174	1.0696
DBH	-0.04004	0.004668	-8.577	-0.05381	-0.02785
CR	1.668	0.05871	28.416	1.468	1.720
PBAL	-0.002556	1.271e-04	-20.105	-0.002739	-0.002222
PRECIP_WIN	4.528e-05	1.87e-06	24.166	3.573e-05	4.970e-05
MAXT10DAYS_WIN	0.001075	2.965e-04	3.626	8.316e-04	0.0023033
MAXT5DAYS_SPR	-0.008998	9.061e-04	-9.931	-0.011070	-0.007050
MINT5DAYS_SUM	0.001887	5.067e-04	3.724	-1.04e-04	0.002587
SLOPE	-0.08127	0.1178	-0.690	-0.28821	0.16395
cos(ASP)*SLOPE	0.05268	0.1022	0.515	-0.14975	0.24029
sin(ASP)*SLOPE	0.1659	0.09784	1.696	0.02525	0.42578
SLOPE*log(ELEV+1)	0.009845	0.01503	0.655	-0.021410	0.036330
SLOPE*log(ELEV+1)* cos(ASP)	-0.006173	0.01298	-0.476	-0.030329	0.019052
SLOPE*log(ELEV+1)* sin(ASP)	-0.02101	0.01247	-1.684	-0.05436	-0.00335
SLOPE*ELEV^2	-4.371e-11	4.074e-10	-0.107	-7.503e-10	8.257e-10
SLOPE*ELEV^2*cos(ASP)	-7.974e-11	3.344e-10	-0.238	-6.902e-10	5.266e-10
SLOPE*ELEV^2*sin(ASP)	4.683e-10	3.345e-10	1.400	3.459e-11	1.379e-09
ELEV	-1.590e-04	1.592e-04	-0.999	-4.096e-04	1.948e-04
ELEV^2	1.208e-08	1.834e-08	0.658	-2.670e-08	4.208e-08
UTMY-E)	1.483e-04	8.546e-05	1.735	-1.259e-04	2.346e-04
UTMY-W	9.469e-05	8.319e-05	1.138	-1.798e-04	1.729e-04

Table S13: Coefficients and statistics for ponderosa pine height growth model.

Parameter	Coefficient	Std Error	t-value	Lower 95% CI	Upper 95% CI
Intercept	3.975	0.6966	5.705	2.3889	4.8907
Log(THT)	0.4151	0.07490	5.543	0.3229	0.6177
THT	-0.005256	0.001137	-4.622	-0.008122	-0.003233
CR	0.9897	0.05764	17.168	0.8790	1.1103
PBAL	-7.145e-04	1.286e-04	-5.554	-0.001016	-5.21e-04
PRECIP_WIN	4.192e-05	3.713e-06	11.290	4.486e-05	6.205e-05
PRECIP_SPRSUM	-9.408e-05	1.033e-05	-9.107	-1.564e-04	-1.088e-04
MAXT10DAYS_WIN	0.002616	3.860e-04	6.778	0.001649	0.003132
MAXT5DAYS_SPR	-0.01740	0.001555	-11.190	-0.01749	-0.01094
MAXT10DAYS_SUM	-0.006085	0.001536	-3.962	-0.007318	-0.001154
SLOPE	-0.3533	0.1164	-3.034	-0.5339	-0.08538
cos(ASP)*SLOPE	-0.07746	0.114	-0.696	-0.2987	0.1055
sin(ASP)*SLOPE	0.1649	0.9615	1.715	-0.0193	0.3519
SLOPE*log(ELEV+1)	0.04375	0.01486	2.945	0.009336	0.066625
SLOPE*log(ELEV+1)*	0.009976	0.01417	0.704	-0.01294	0.03823

cos(ASP)					
SLOPE*log(ELEV+1)* sin(ASP)	-0.02087	0.01226	-1.703	-0.04385	0.00380
SLOPE*ELEV^2	-6.587e-10	4.049e-10	-1.627	-1.329e-09	2.519e-10
SLOPE*ELEV^2*cos(ASP)	-3.704e-10	3.774e-10	-0.981	-1.109e-09	2.352e-10
SLOPE*ELEV^2*sin(ASP)	4.896e-10	3.275e-10	1.495	-1.773e-10	1.069e-09
ELEV	-3.338e-04	1.533e-04	-2.178	-5.796e-05	1.65e-05
ELEV^2	1.919e-08	1.777e-08	1.080	-2.176e-08	4.611e-08
UTMY-E	-6.761e-04	8.464e-05	-7.988	-8.462e-04	-5.162e-04
UTMY-W	-6.279e-04	8.617e-05	-7.287	-8.862e-04	-5.662e-04

Table S14: Coefficients and statistics for sugar pine diameter growth model.

Parameter	**Coefficient**	**Std Error**	**t-value**	**Lower 95% CI**	**Upper 95% CI**
Intercept	0.3692	1.142	0.323	-0.4736	4.5222
Log(DBH)	0.9975	0.1020	9.77	0.6899	1.2554
DBH	-0.03065	0.005976	-5.130	-0.04967	-0.01942
CR	1.746	0.09927	17.594	1.576	1.936
PBAL	-0.001816	1.787e-04	-10.163	-0.001928	-0.001177
PRECIP_WIN	2.387e-05	3.05e-06	7.820	1.699e-05	3.458e-05
MINT5DAYS_WIN	-0.007414	0.001206	-6.148	-0.007903	-0.002095
MINT5DAYS_SPR	0.002929	0.001085	2.699	-5.54e-04	0.004755
MINT5DAYS_SUM	0.001927	6.806e-04	2.832	2.73e-04	0.003231
SLOPE	-0.5925	0.2174	-2.726	-1.0078	-0.2150
cos(ASP)*SLOPE	-0.02295	0.1371	-0.167	-0.3366	0.1743
sin(ASP)*SLOPE	0.3074	0.1999	1.538	0.1265	0.8924
SLOPE*log(ELEV+1)	0.07328	0.02761	2.654	-0.02540	0.12640
SLOPE*log(ELEV+1)* cos(ASP)	0.003423	0.01735	0.197	-0.020793	0.043794
SLOPE*log(ELEV+1)* sin(ASP)	-0.03821	0.02526	-1.513	-0.11160	-0.01503
SLOPE*ELEV^2	-1.278e-09	7.132e-10	-1.792	-2.526e-09	7.228e-11
SLOPE*ELEV^2*cos(ASP)	-2.520e-10	4.197e-10	-0.600	-1.393e-09	2.159e-10
SLOPE*ELEV^2*sin(ASP)	7.017e-10	6.123e-10	1.146	-1.251e-10	2.177e-09
ELEV	-9.987e-04	3.750e-04	-2.663	-0.001863	-4.698e-04
ELEV^2	8.991e-08	4.132e-08	2.152	2.545e-08	1.763e-07
UTMY	-6.129e-04	1.517e-04	-4.040	-0.0012114	-5.819e-04

Table S15: Coefficients and statistics for sugar pine height growth model.

Parameter	Coefficient	Std Error	t-value	Lower 95% CI	Upper 95% CI
Intercept	0.4644	1.131	0.411	-1.8552	2.5493
Log(THT)	0.2880	0.1261	2.284	0.0385	0.5651
THT	-0.004868	0.001837	-2.650	-0.008808	-0.001109
CR	0.6394	0.1013	6.315	0.4147	0.8110
PBAL	-9.977e-04	1.872e-04	-5.328	-0.001467	-7.357e-04
PRECIP_SPRSUM	-3.416e-05	1.148e-05	-2.976	-6.473e-05	2.129e-05
MINT5DAYS_SPR	0.004991	0.001248	4.000	0.002468	0.007245
MINT10DAYS_WIN	-0.02387	0.009346	-2.554	-0.04592	-0.00900
SLOPE	0.3154	0.2173	1.452	-0.0678	0.7353
cos(ASP)*SLOPE	-0.2623	0.1407	-1.864	-0.5534	-0.0113
sin(ASP)*SLOPE	0.3033	0.1976	1.535	-0.0803	0.6995
SLOPE*log(ELEV+1)	-0.04019	0.02764	-1.454	-0.09347	0.00853
SLOPE*log(ELEV+1)* cos(ASP)	0.03354	0.01787	1.878	0.00197	0.07118
SLOPE*log(ELEV+1)* sin(ASP)	-0.03870	0.02502	-1.547	-0.08766	0.01070
SLOPE*ELEV^2	1.123e-09	7.324e-10	1.533	-3.035e-10	2.398e-09
SLOPE*ELEV^2*cos(ASP)	-8.692e-10	4.555e-10	-1.908	-1.782e-09	-2.178e-11
SLOPE*ELEV^2*sin(ASP)	1.022e-09	6.236e-10	1.638	-1.816e-10	2.234e-09
ELEV	5.561e-04	3.774e-04	1.474	-1.553e-04	0.0013123
ELEV^2	-6.816e-08	4.214e-08	-1.617	-1.574e-07	8.886e-09
UTMY-E	-5.903e-04	1.488e-04	-4.644	-8.896e-04	-2.972e-04
UTMY-W	-6.907e-04	1.536e-04	-3.842	-9.864e-04	-4.147e-04

Table S16: Coefficients and statistics for incense-cedar diameter growth model.

Parameter	Coefficient	Std Error	t-value	Lower 95% CI	Upper 95% CI
Intercept	-6.056	0.8877	-6.822	-7.9699	-4.7425
Log(DBH)	0.8138	0.08088	10.062	0.6120	1.0752
DBH	-0.03931	0.005318	-7.392	-0.05528	-0.02987
CR	1.566	0.06571	23.830	1.495	1.794
PBAL	-0.002262	1.294e-04	-17.481	-0.002333	-0.001738
PRECIP_WIN	3.957e-05	2.64e-06	14.989	3.145e-05	4.425e-05
PRECIP_SUM	-1.912e-04	4.038e-05	-4.736	-2.403e-04	-7.21e-05
MAXT5DAYS_SUM	0.006097	0.001284	4.748	0.002593	0.008008
MAXT5DAYS_SPR	-0.004008	0.001235	-3.246	-0.009028	-0.002611
MINT5DAYS_WIN	-0.005188	8.676e-04	-5.980	-0.006029	-0.002469
SLOPE	-0.3133	0.1832	-1.710	-0.6189	0.0577
cos(ASP)*SLOPE	-0.5097	0.1593	-3.199	-0.7595	-0.1408
sin(ASP)*SLOPE	0.2554	0.1396	1.829	0.0756	0.6253
SLOPE*log(ELEV+1)	0.03900	0.02320	1.681	-0.007806	0.07825
SLOPE*log(ELEV+1)* cos(ASP)	0.06456	0.02015	3.205	-0.01865	0.09663

SLOPE*log(ELEV+1)* sin(ASP)	-0.03268	0.01771	-1.845	-0.800	-0.0101
SLOPE*ELEV^2	-7.495e-10	5.766e-10	-1.300	-1.6809e-09	4.9805e-10
SLOPE*ELEV^2*cos(ASP)	-1.410e-09	4.914e-10	-2.869	-2.2800e-09	-4.1083e-10
SLOPE*ELEV^2*sin(ASP)	9.246e-10	4.495e-10	2.057	2.316e-10	1.9992e-09
ELEV	-4.607e-04	2.454e-04	-1.878	-1.1644e-03	-1.2835e-04
ELEV^2	4.492e-08	2.681e-08	1.676	7.8700e-09	1.2114e-07
UTMY-E	5.561e-04	1.370e-04	4.058	4.675e-04	0.0010000
UTMY-W	5.234e-04	1.307e-04	4.004	4.340e-04	9.440e-04

Table S17: Coefficients and statistics for incense-cedar height growth model.

Parameter	**Coefficient**	**Std Error**	**t-value**	**Lower 95% CI**	**Upper 95% CI**
Intercept	1.612	0.8982	1.795	-0.539	3.192
Log(THT)	0.3858	0.09915	3.891	0.232	0.635
THT	-0.005053	0.001997	-2.530	-0.00976	-0.00162
CR	0.6853	0.06387	10.730	0.5785	0.8191
PBAL	-9.358e-04	1.256e-04	-7.451	-0.001239	-7.59e-04
PRECIP_WIN	2.375e-05	3.632e-06	6.539	1.783e-05	3.202e-05
MINT5DAYS_WIN	-0.005851	0.001083	-5.401	-0.008379	-0.003837
MAXT5DAYS_SPR	-0.01486	0.002143	-6.931	-0.01880	-0.00105
TMAX_SUM	3.310e-04	5.96e-05	5.555	2.448e-04	4.768e-04
SLOPE	-0.07336	0.1805	-0.406	-0.4085	0.2704
cos(ASP)*SLOPE	-0.4239	0.1605	-2.640	-0.7177	-0.1079
sin(ASP)*SLOPE	0.2043	0.1361	1.501	-0.0797	0.4682
SLOPE*log(ELEV+1)	0.009298	0.02288	0.406	-0.03422	0.05184
SLOPE*log(ELEV+1)* cos(ASP)	0.05250	0.02035	2.580	0.01215	0.08957
SLOPE*log(ELEV+1)* sin(ASP)	-0.02617	0.01728	-1.515	-0.05969	0.00975
SLOPE*ELEV^2	-2.222e-10	5.825e-10	-0.381	-1.310e-09	8.204e-10
SLOPE*ELEV^2*cos(ASP)	-8.086e-10	5.158e-10	-1.568	-1.822e-09	1.056e-10
SLOPE*ELEV^2*sin(ASP)	6.922e-10	4.453e-10	1.555	-1.276e-10	1.671e-09
ELEV	1.649e-04	2.348e-04	0.702	-2.499e-04	6.570e-04
ELEV^2	-2.081e-08	2.590e-08	-0.803	-7.464e-08	2.181e-08
UTMY	-8.243e-04	1.171e-04	-7.041	-0.001065	-5.78e-04

Table S18: Coefficients and statistics for white fir diameter growth model.

Parameter	**Coefficient**	**Std Error**	**t-value**	**Lower 95% CI**	**Upper 95% CI**
Intercept	-6.974	0.4902	-14.23	-7.8897	-5.4505
Log(DBH)	0.9526	0.05205	18.30	0.6827	1.1774
DBH	-0.04723	0.003660	-12.91	-0.06276	-0.03475
CR	1.798	0.03654	49.19	1.672	1.848
PBAL	-0.001945	1.488e-05	-25.98	-0.002047	-0.001690

PRECIP_WINSPR	3.066e-05	1.269e-06	24.15	2.150e-04	3.440e-05
PRECIP_SUM	-3.520e-04	2.377e-05	-14.81	-4.034e-04	-2.325e-04
MAXT5DAYS_SUM	0.006387	0.001052	6.07	0.002548	0.008607
MAXT10DAYS_SPR	-0.003861	3.807e-04	-10.14	-0.004742	-0.002737
MINT5DAYS_WIN	0.002543	3.496e-04	7.27	0.002232	0.004290
SLOPE	0.2771	0.1021	2.71	0.0449	0.4378
cos(ASP)*SLOPE	0.02515	0.07853	0.32	-0.1388	0.1677
sin(ASP)*SLOPE	0.07727	0.08940	0.86	-0.1408	0.2072
SLOPE*log(ELEV+1)	-0.03476	0.01276	-2.72	-0.05504	-0.00575
SLOPE*log(ELEV+1)* cos(ASP)	-0.002830	0.009761	-0.29	-0.02085	0.01722
SLOPE*log(ELEV+1)* sin(ASP)	-0.009364	0.01121	-0.84	-0.02561	0.01780
SLOPE*ELEV^2	6.287e-10	2.568e-10	2.45	-7.666e-11	1.070e-09
SLOPE*ELEV^2*cos(ASP)	-6.046e-11	1.817e-10	-0.33	-3.965e-10	2.956e-10
SLOPE*ELEV^2*sin(ASP)	1.263e-10	2.085e-10	0.61	-3.644e-10	4.502e-10
ELEV	1.633e-04	1.083e-04	1.51	-5.880e-05	3.512e-04
ELEV^2	-1.949e-08	1.100e-08	-1.77	-3.458e-08	8.405e-09
UTMY-E	3.147e-04	6.815e-05	4.62	1.003e-04	4.165e-04
UTMY-W	2.771e-04	6.591e-05	4.20	6.304e-05	3.741e-04

Table S19: Coefficients and statistics for white fir height growth model.

Parameter	**Coefficient**	**Std Error**	**t-value**	**Lower 95% CI**	**Upper 95% CI**
Intercept	-0.2586	0.5033	-0.514	-1.013	1.087
Log(THT)	0.5446	0.06675	8.158	0.3961	0.6538
THT	-0.008433	0.001089	-7.732	-0.01055	-0.006238
CR	1.009	0.04060	24.846	0.9161	1.0778
PBAL	-0.001175	8.280e-05	-14.186	-0.001438	-0.001103
PRECIP_WIN	2.028e-05	2.27e-06	8.925	1.472e-05	2.348e-05
TMAX_WIN	-5.535e-04	8.27e-05	-6.691	-0.001679	-8.984e-04
TMAX_SPR	1.689e-04	5.04e-05	3.350	2.404e-04	0.001028
TMAX_SUM	1.273e-04	4.269e-05	2.983	1.978e-04	6.891e-04
MAXT5DAYS	0.002741	5.845e-04	4.690	0.001219	0.003527
ELEV	-8.396e-05	1.263e-05	-6.650	-1.121e-04	-6.455e-05
UTMY-E	-6.083e-04	7.77e-05	-7.822	-8.140e-04	-4.941e-04
UTMY-W	-6.374e-04	7.598e-05	-8.390	-8.394e-04	-5.333e-04

Table S20: Coefficients and statistics for red fir diameter growth model.

Parameter	**Coefficient**	**Std Error**	**t-value**	**Lower 95% CI**	**Upper 95% CI**
Intercept	0.3728	1.334	0.28	-2.9402	2.0344
Log(DBH)	0.8458	0.07218	11.72	0.6248	1.1743
DBH	-0.04054	0.004527	-8.96	-0.05761	-0.03294
CR	2.199	0.06894	31.90	1.977	2.265

PBAL	-5.433e-04	1.407e-04	-3.86	-8.653e-04	-1.685e-04
PRECIP_WIN	1.198e-05	3.24e-06	3.70	1.225e-06	1.556e-05
PRECIP_SUM	-2.205e-04	2.948e-05	-7.48	-2.611e-04	-1.338e-04
MAXT10DAYS_WIN	-0.003764	7.079e-04	-5.32	-0.004953	-0.001896
MAXT5DAYS_SPR	-0.005287	0.001231	-4.29	-0.007447	-0.002230
MAXT10DAYS_SUM	-0.01329	0.003802	-3.50	-0.02772	-0.00670
SLOPE	-0.1710	0.3486	-0.49	-0.8614	0.4178
cos(ASP)*SLOPE	0.4345	0.2123	2.05	-0.0999	0.7443
sin(ASP)*SLOPE	0.1015	0.3041	0.33	-0.7026	0.5356
SLOPE*log(ELEV+1)	0.02109	0.4223	0.5.	-0.04906	-0.10592
SLOPE*log(ELEV+1)* cos(ASP)	-0.05356	0.02560	-2.09	-0.08925	0.01263
SLOPE*log(ELEV+1)* sin(ASP)	-0.01196	0.03668	-0.33	-0.06444	0.08440
SLOPE*ELEV^2	-2.502e-10	5.187e-10	-0.48	-1.240e-09	6.649e-10
SLOPE*ELEV^2*cos(ASP)	7.289e-10	2.881e-10	2.53	-6.077e-12	1.45e-09
SLOPE*ELEV^2*sin(ASP)	4.412e-11	4.188e-10	0.11	-9.912e-10	6.560e-10
ELEV	-4.076e-04	3.610e-04	-1.13	-8.762e-04	4.224e-04
ELEV^2	2.225e-8	2.817e-08	0.79	-3.034e-08	6.992e-08
UTMY	2.222e-04	9.227e-05	-2.41	-3.074e-04	1.985e-04

Table S21: Coefficients and statistics for red fir height growth model.

Parameter	**Coefficient**	**Std Error**	**t-value**	**Lower 95% CI**	**Upper 95% CI**
Intercept	-0.6212	1.419	-0.438	-3.077	2.0785
Log(THT)	0.8883	0.07821	11.358	0.7212	1.032
THT	-0.01286	0.001655	-7.771	-0.01566	-0.00909
CR	1.625	0.08606	18.886	1.447	1.787
PRECIP_SPR	-3.361e-05	1.224e-05	-2.745	-5.675e-05	-1.056e-05
MAXT10DAYS_WIN	-0.004863	0.001144	-4.249	-0.006940	-0.002544
SLOPE	-0.09940	0.3899	-0.255	-0.7639	0.7273
cos(ASP)*SLOPE	0.6787	0.2624	2.587	0.1714	1.1707
sin(ASP)*SLOPE	-0.5635	0.3331	-1.691	-1.1958	0.0442
SLOPE*log(ELEV+1)	0.01090	0.04746	0.230	-0.08963	0.09208
SLOPE*log(ELEV+1)* cos(ASP)	-0.08301	0.03174	-2.616	-0.14175	-0.02046
SLOPE*log(ELEV+1)* sin(ASP)	0.06796	0.04039	1.683	-0.00478	0.14496
SLOPE*ELEV^2	2.375e-10	6.324e-10	0.376	-8.714e-10	1.571e-09
SLOPE*ELEV^2*cos(ASP)	1.048e-09	3.766e-10	2.784	3.811e-10	1.806e-09
SLOPE*ELEV^2*sin(ASP)	-7.426e-10	5.042e-10	-1.473	-1.704e-09	1.820e-10
ELEV	-2.045e-06	4.187e-04	-0.005	-7.892e-04	7.703e-04
ELEV^2	-1.865e-08	3.375e-08	-0.552	-7.996e-08	4.494e-08
UTMY	-4.853e-04	1.254e-04	-3.870	-7.387e-04	-2.542e-04

Figure S1: Plot locations in mixed-conifer forest in the Lake Tahoe Basin, California. Each symbol represents a plot location. Symbols vary by drainage location.

Values for climate parameters from the A2 emission scenario by GCM that are included in the height and diameter growth models are presented in Figures S2-S12.

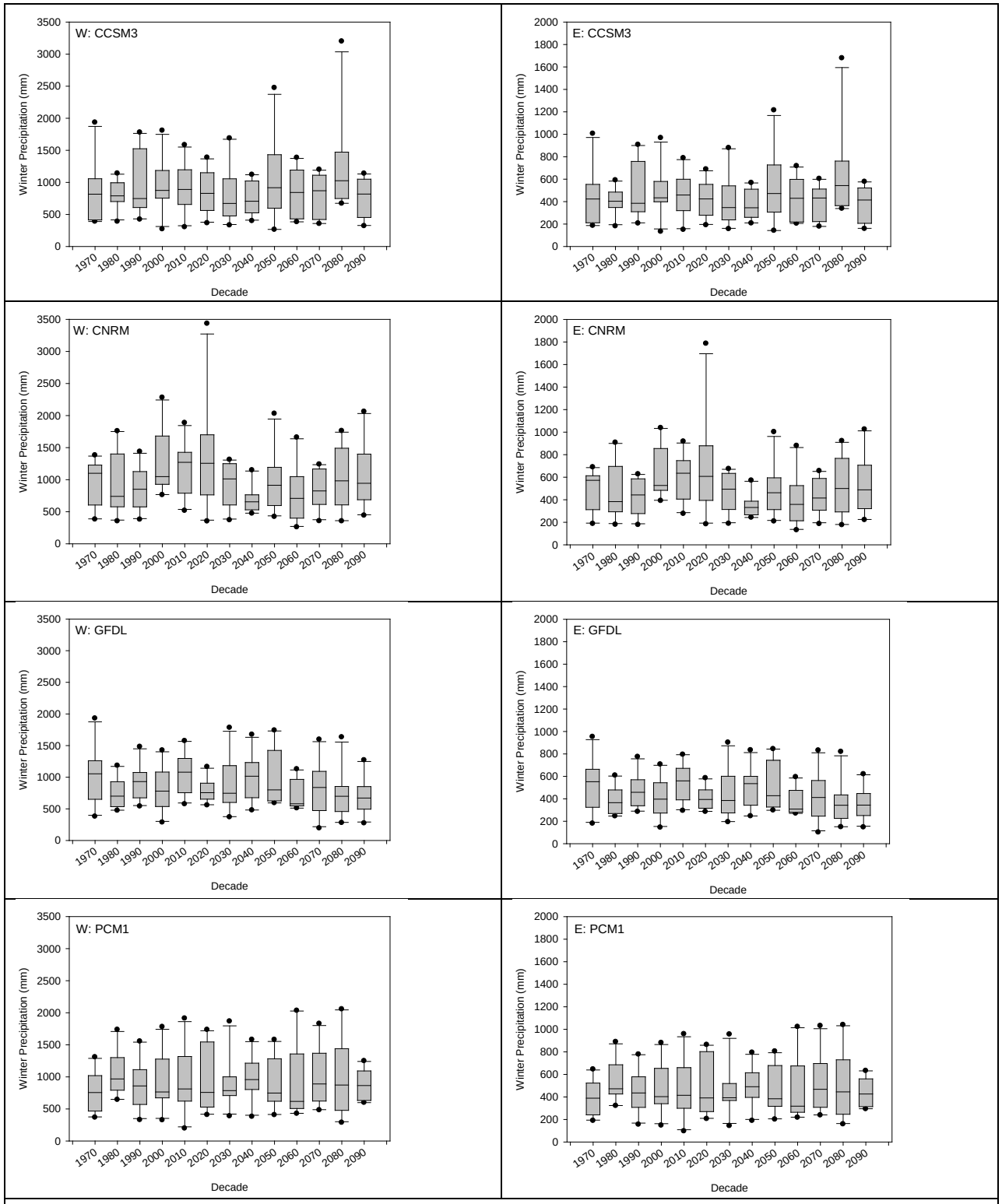

Supplementary Figure S2: Downscaled winter precipitation by Global Climate Model by decade for the western (left column) and eastern (right column) sides of the Lake Tahoe Basin. The y-axis scale differs between east and west.

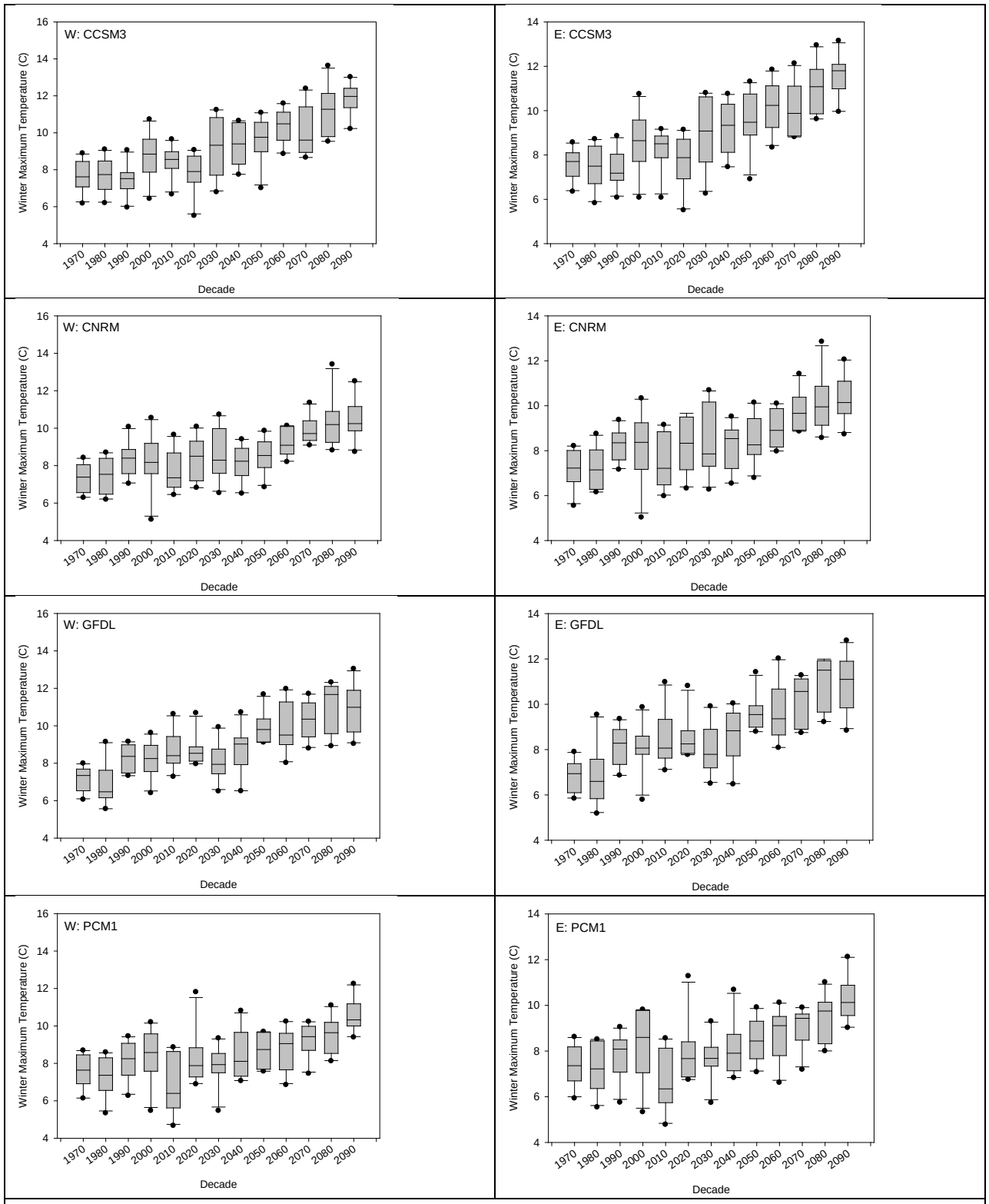

Supplementary Figure S3: Downscaled winter maximum temperature by Global Climate Model by decade for the western (left column) and eastern (right column) sides of the Lake Tahoe Basin. The y-axis scale differs between east and west.

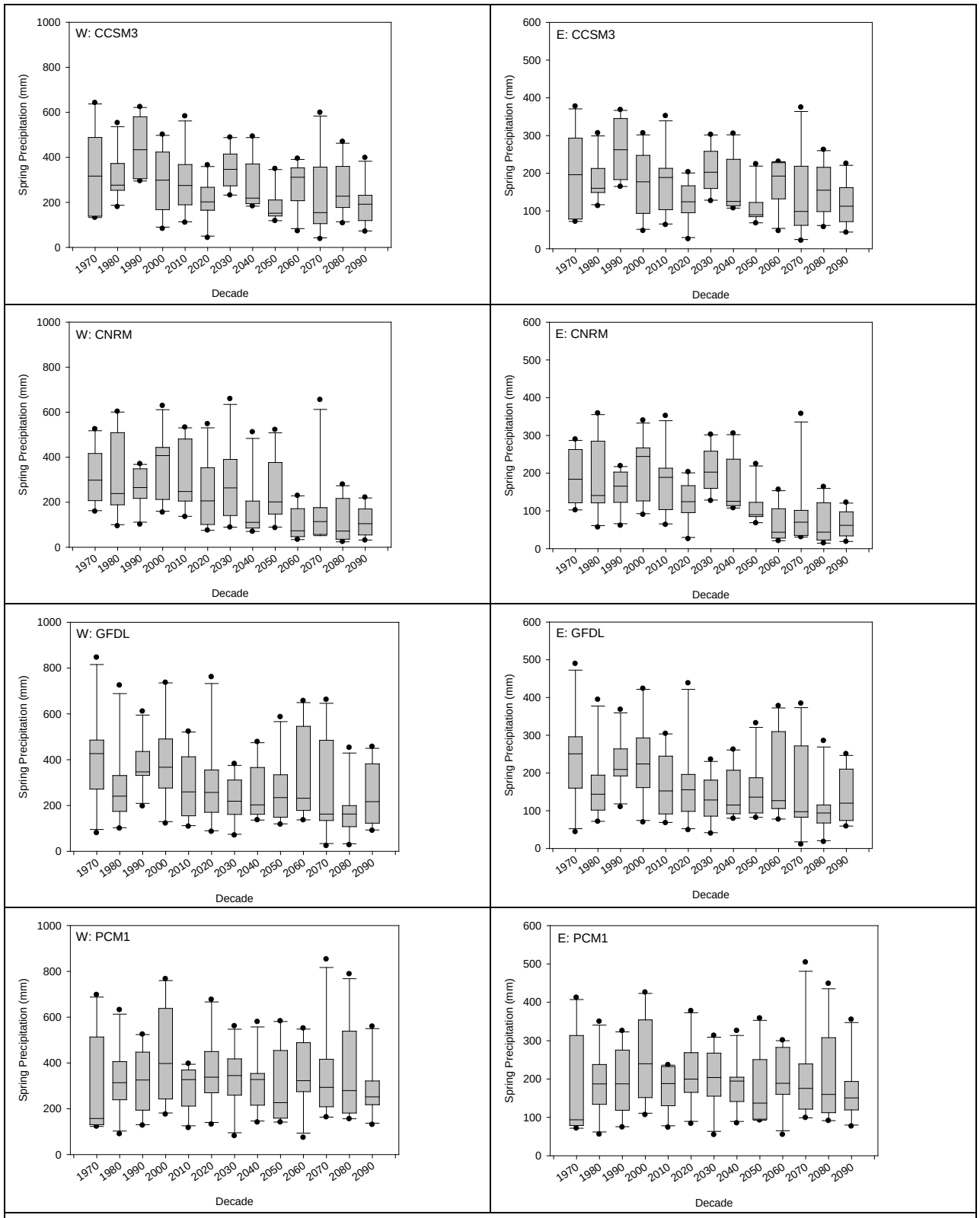

Supplementary Figure S4: Downscaled spring precipitation by Global Climate Model by decade for the western (left column) and eastern (right column) sides of the Lake Tahoe Basin. The y-axis scale differs between east and west.

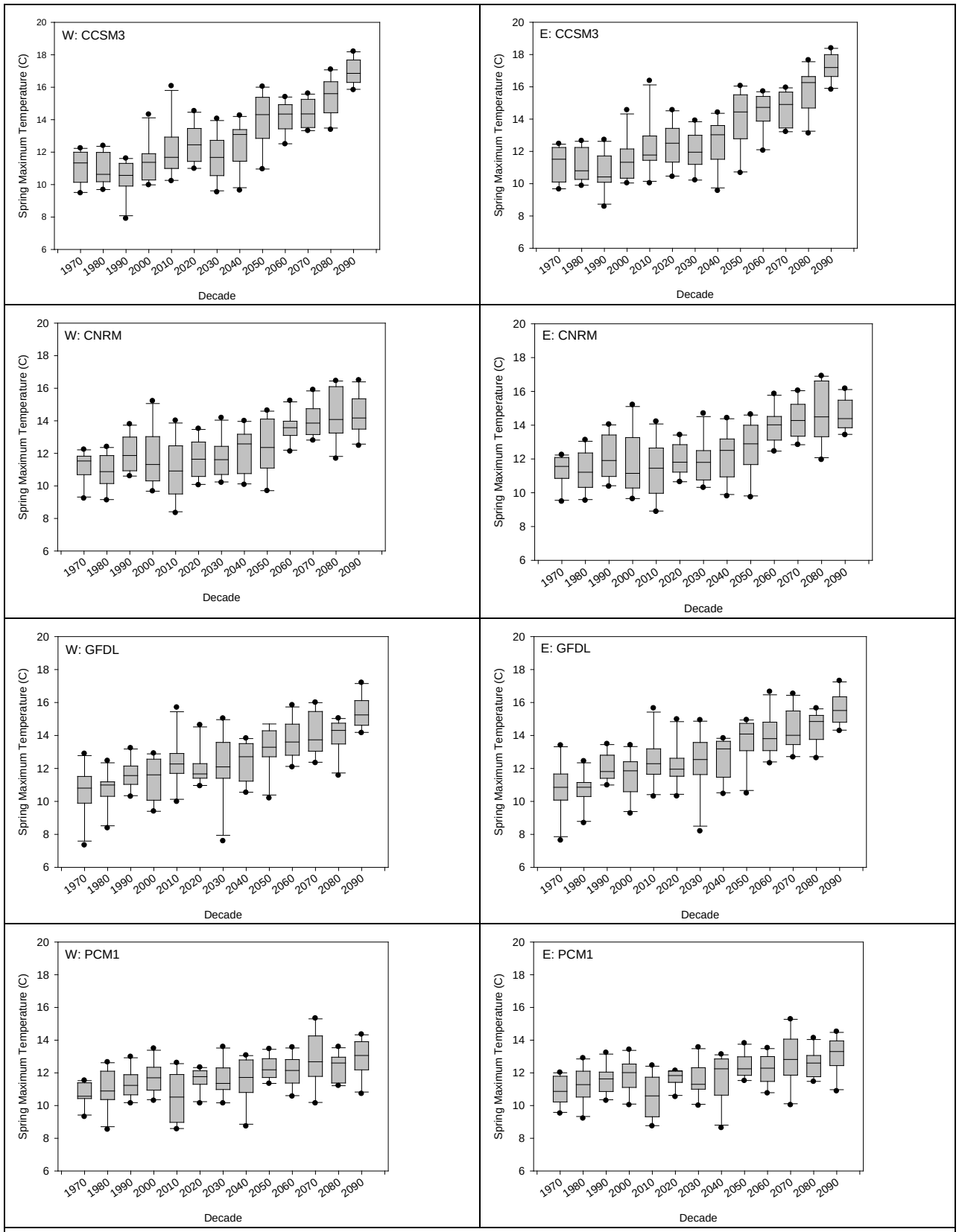

Supplementary Figure S5: Downscaled spring maximum temperature by Global Climate Model by decade for the western (left column) and eastern (right column) sides of the Lake Tahoe Basin.

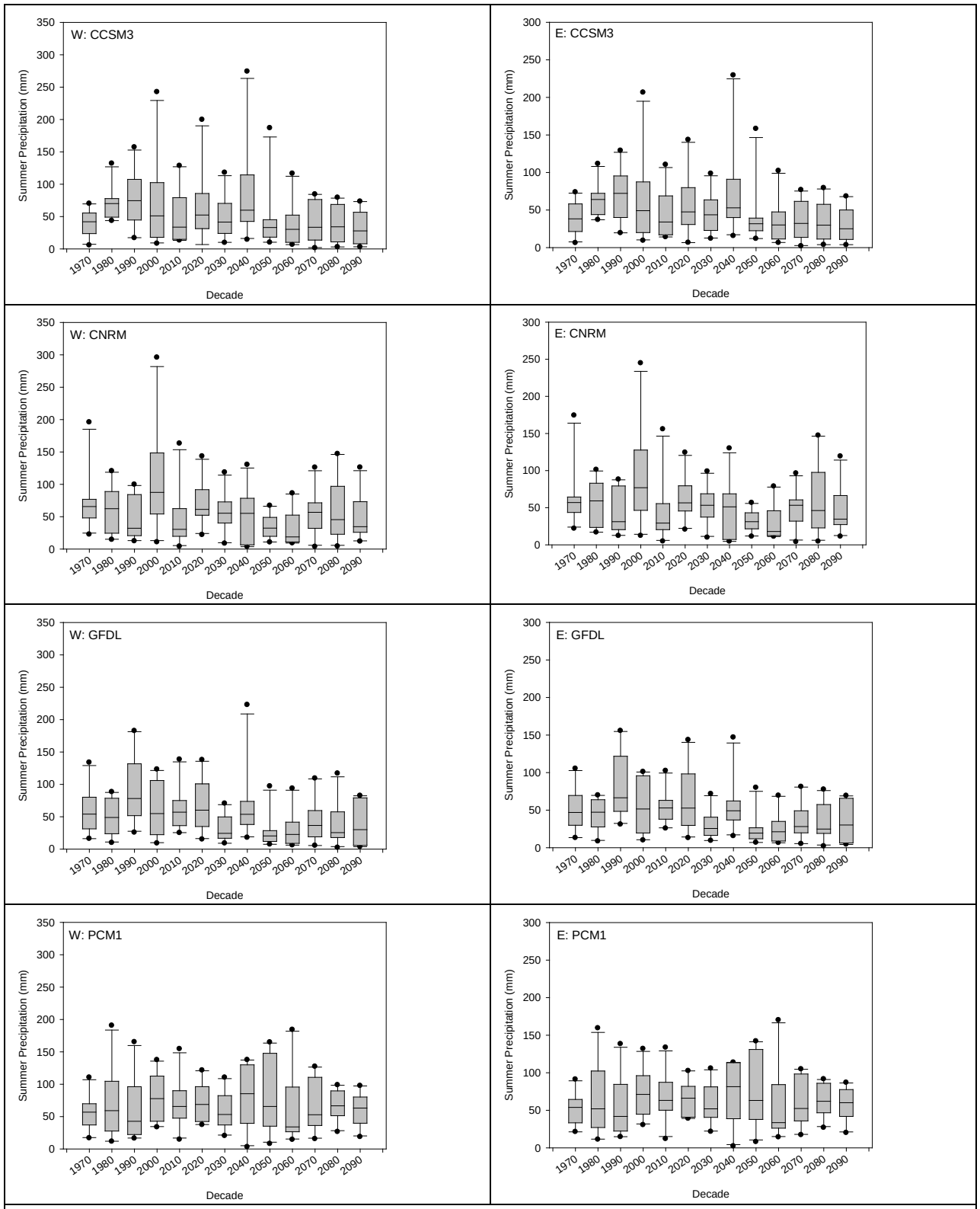

Supplementary Figure S6: Downscaled summer precipitation by Global Climate Model by decade for the western (left column) and eastern (right column) sides of the Lake Tahoe Basin. The y-axis scale differs between east and west.

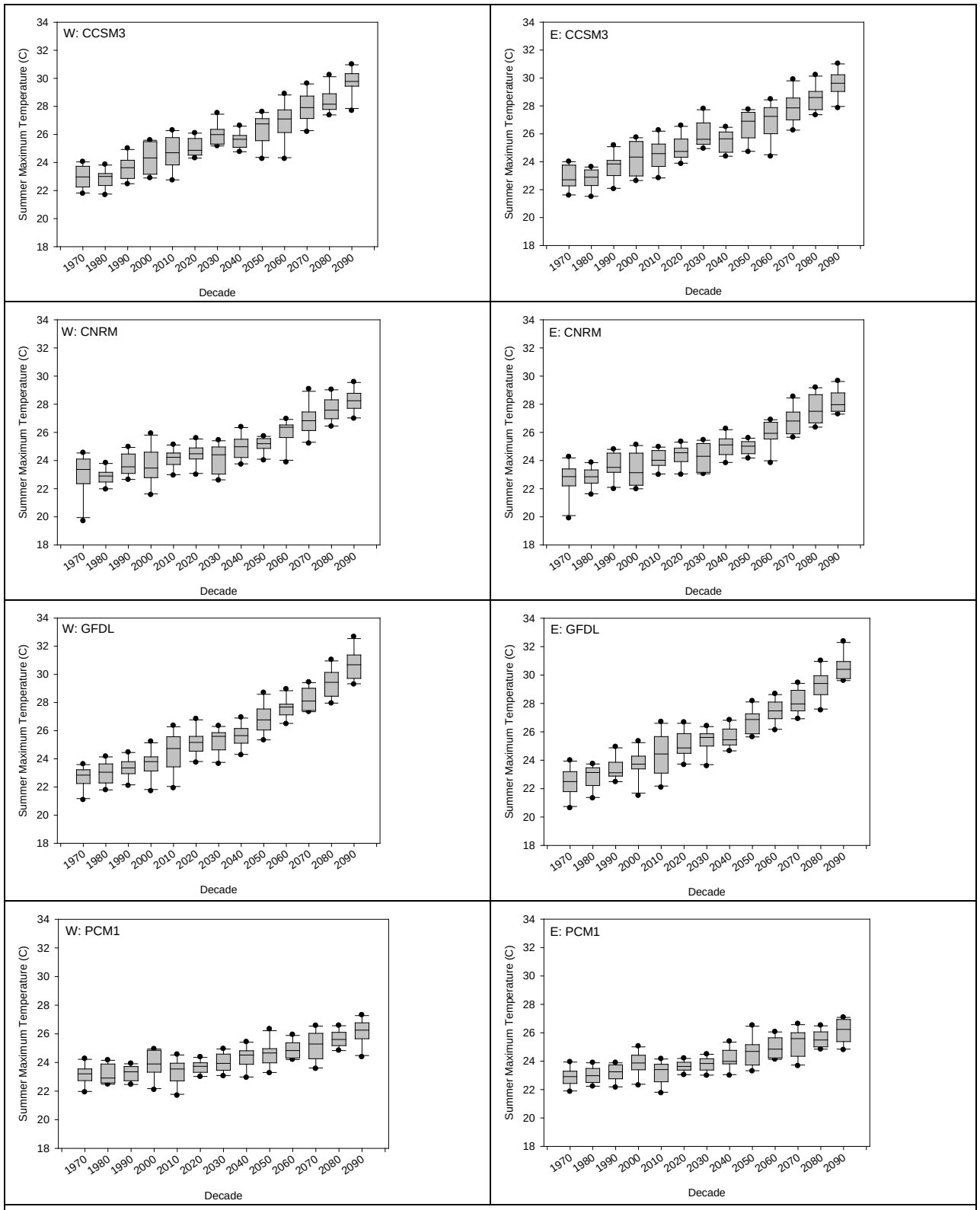

Supplementary Figure S7: Downscaled summer maximum temperature by Global Climate Model by decade for the western (left column) and eastern (right column) sides of the Lake Tahoe Basin.

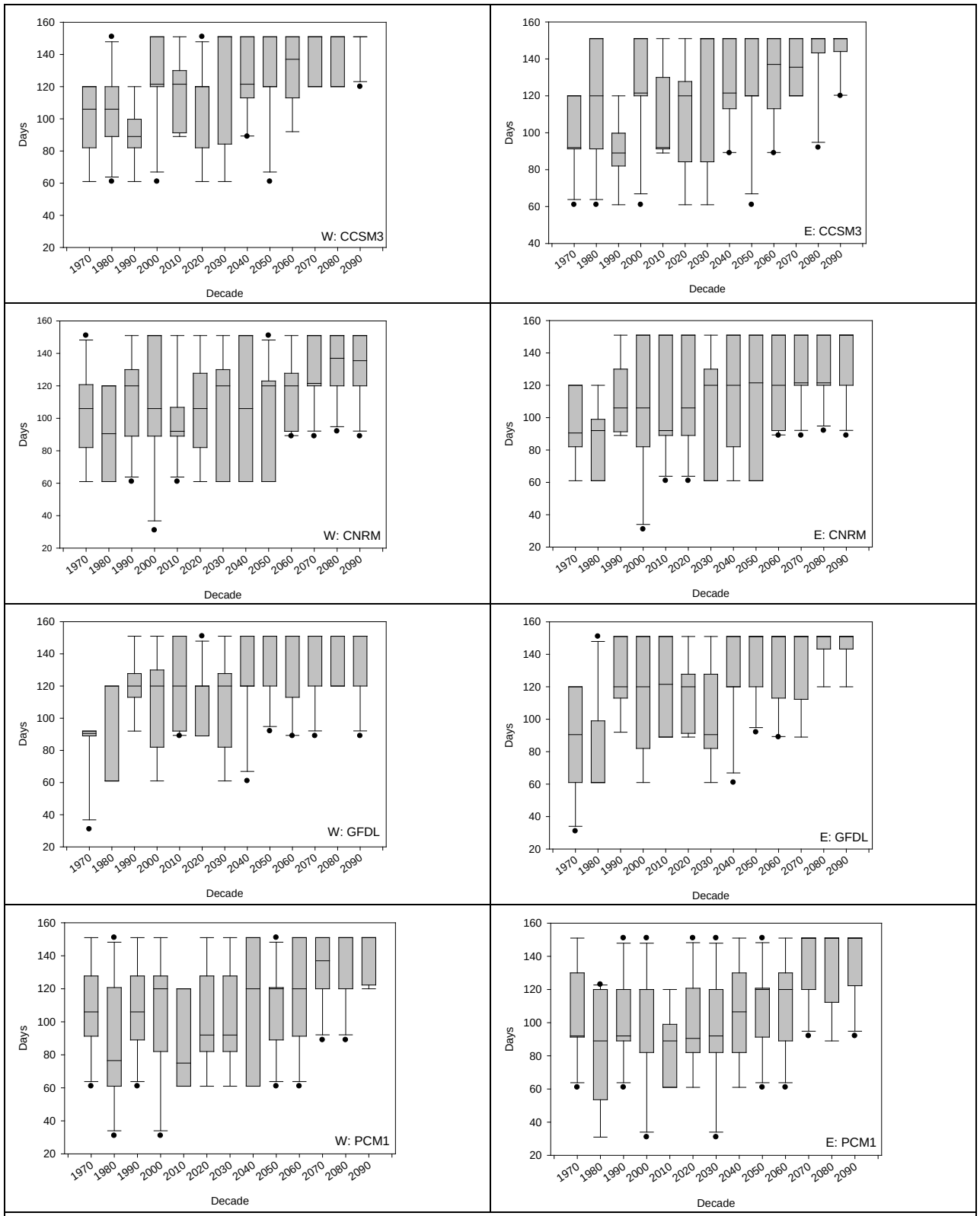

Supplementary Figure S8: Number of days with winter mean daily maximum temperature above 5°C by decade for the western (left column) and eastern (right column) sides of the Lake Tahoe Basin. The y-axis scale differs between east and west.

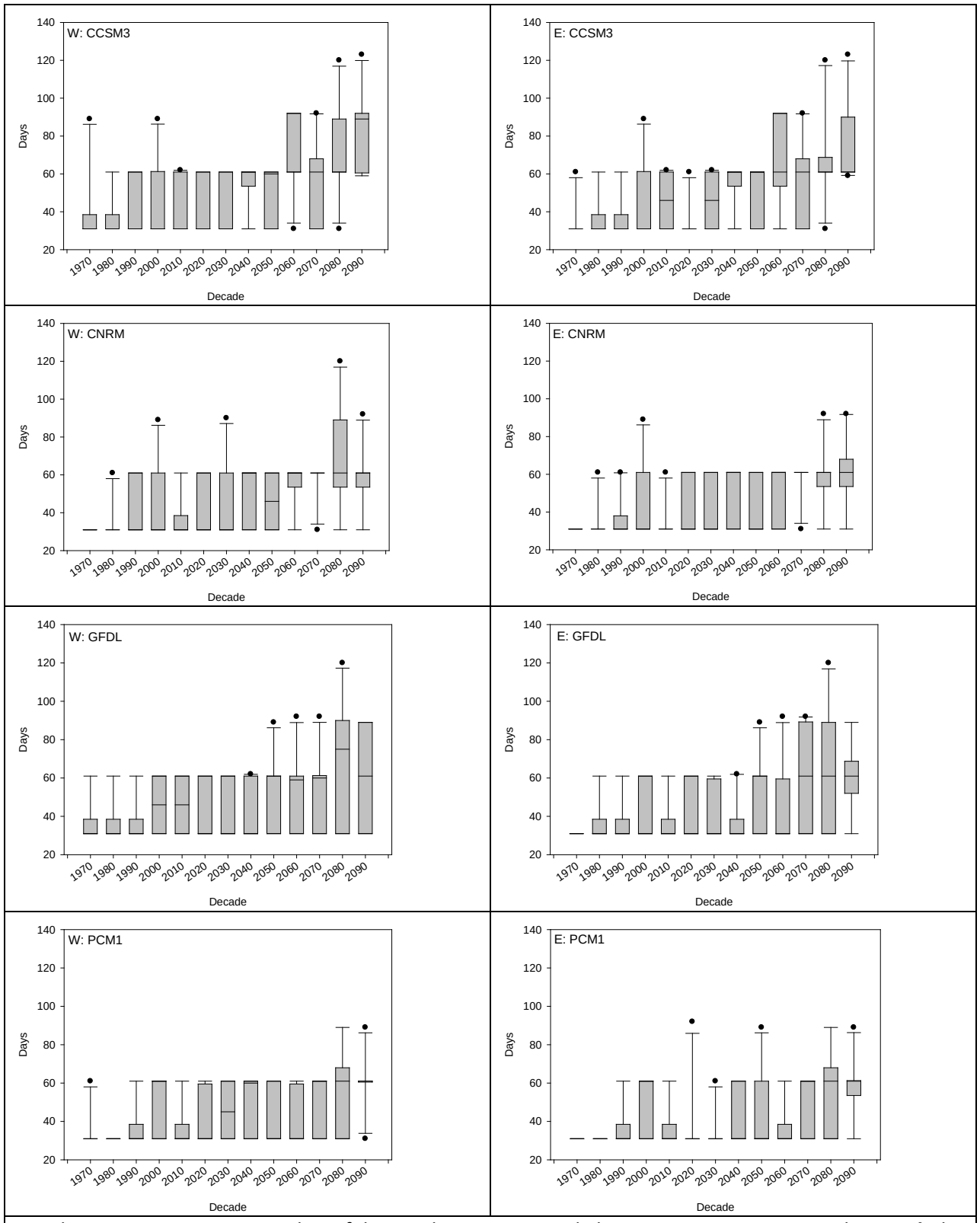

Supplementary Figure S9: Number of days with winter mean daily maximum temperature above 10°C by decade for the western (left column) and eastern (right column) sides of the Lake Tahoe Basin.

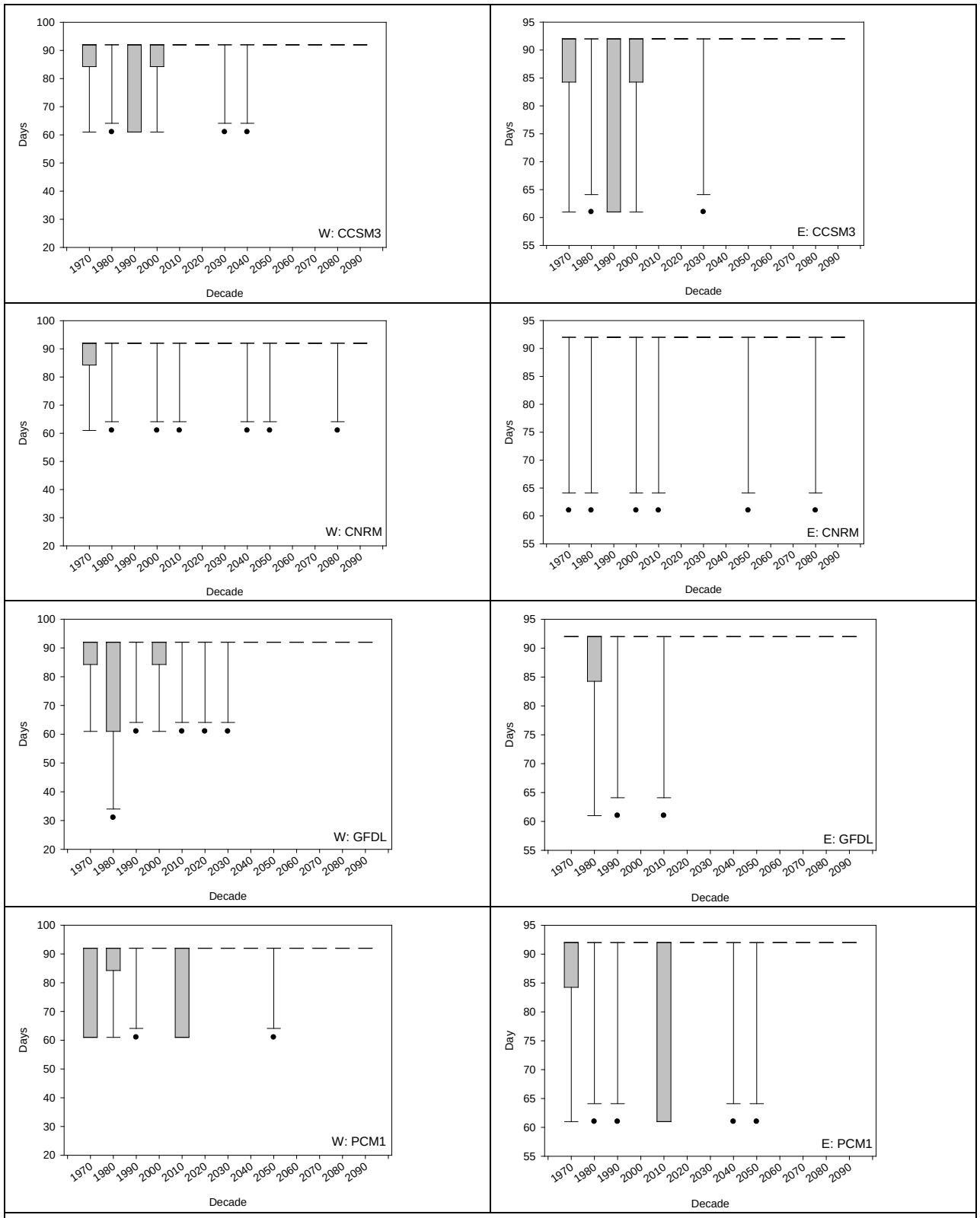

Supplementary Figure S10: Number of days with spring mean daily maximum temperature above 5°C by decade for the western (left column) and eastern (right column) sides of the Lake Tahoe Basin. The y-axis scale differs between east and west.

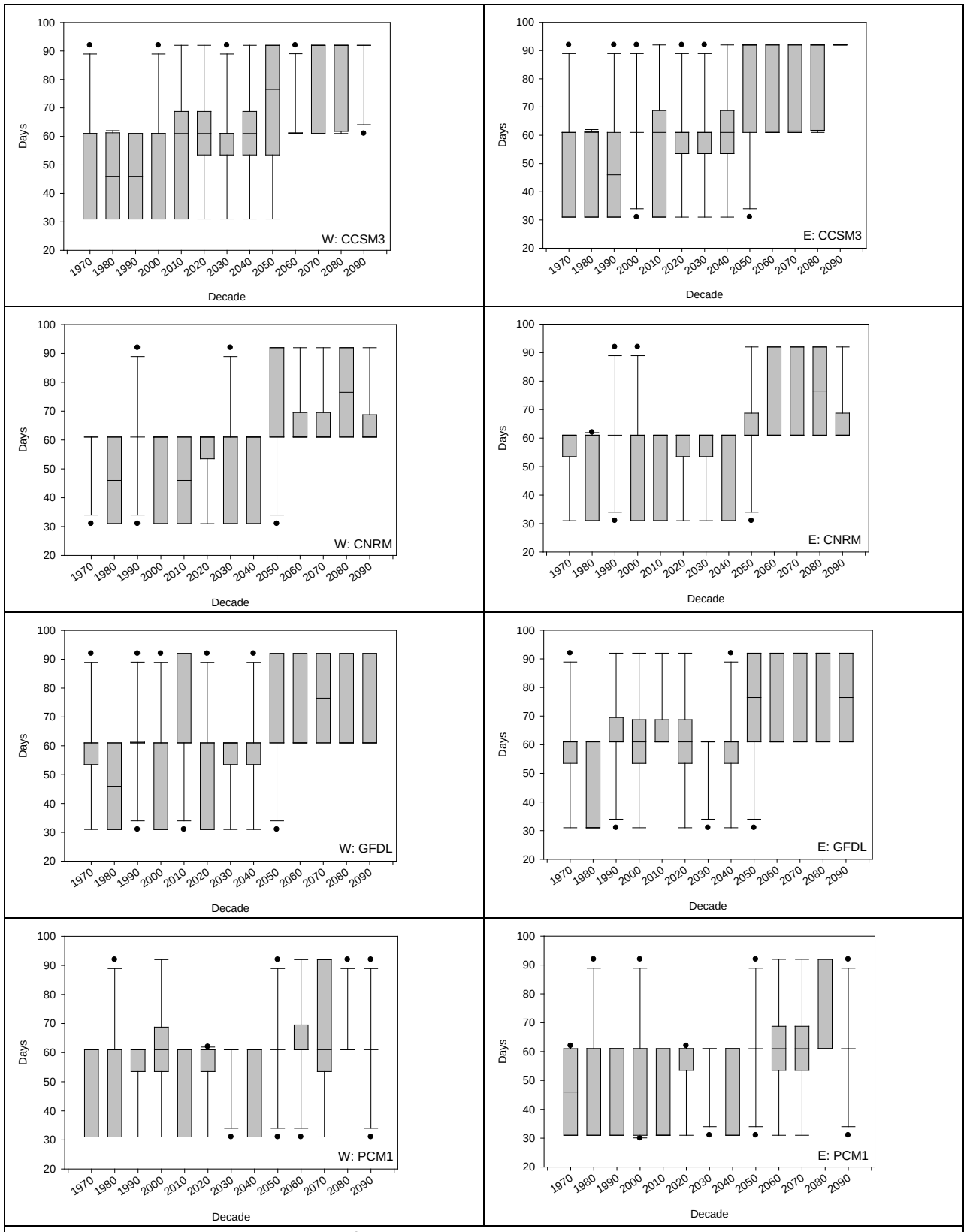

Supplementary Figure S11: Number of days with spring mean daily maximum temperature above 10°C by decade for the western (left column) and eastern (right column) sides of the Lake Tahoe Basin.

Supplemental Material References

Biging, G.S. 1983. Stem analysis procedures for use in obtaining time series forest growth data. Northern California Forest Yield Coop Research Note, University of California, Berkeley 6:46.

Dolph, K.L. 1988. Predicting height increment of young-growth mixed conifers in the Sierra Nevada. USDA Forest Service Research Paper, PSW-RP-191:7.

Dolph, K.L. 1992. A diameter increment model for red fir in California and Southern Oregon. USDA Forest Service Research Paper, PSW-RP-210:6.

Dolph, K.L. and E.L. Amidon. 1979. Predicting growth of mixed-conifer species in the Sierra Nevada: rationale and methods. USDA Forest Service Research Note, PSW-RP-339:7.